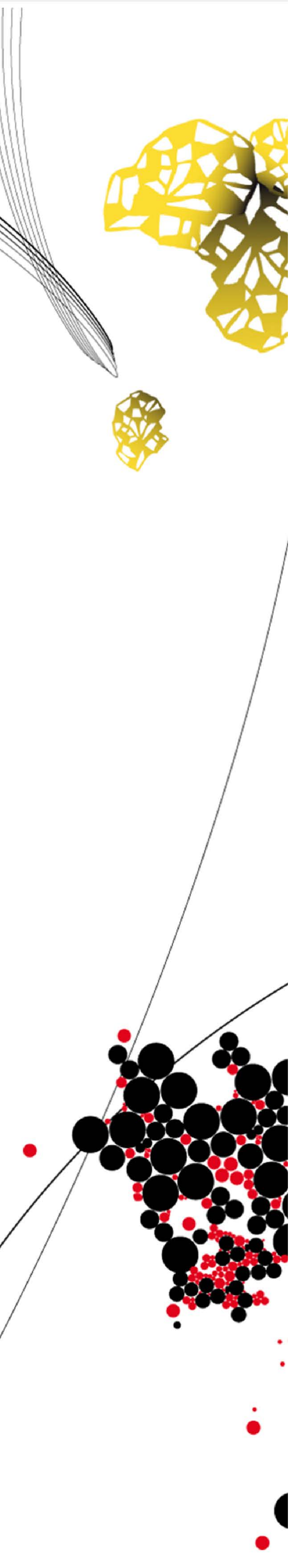

UNIVERSITY OF TWENTE.

Faculty of Mechanical Engineering,
Maintenance & Operations

Surface wettability investigation of the CVT components

Yawar Abbas
Internship report January 2018

Supervisors: Walter Goorts
Houcine Dhieb

Summary

A step wise approach is followed in this report. First, the governing principle of a wetting behavior is explained followed by the key factors that play a role in wetting behavior of a liquid when it encounters a certain surface. Then the wettability of CVT components are determined by performing contact angle measurements. Considering results obtained from the contract angle measurements the contact with maximum potential of improvement from wettability point of view is chosen for surface modification. Different surface modification techniques are explored and after through literature study and taking into consideration the operating conditions of the CVT belt EDM technique is proposed to construct the desired surface geometry on the test specimen. It is also recommended to explore suitable surface coatings in the future that can be used on top of the constructed surface geometry to achieve a robust wetting behavior.

The design parameters for the desired surface geometry are carefully chosen after thorough investigation of the key parameters required for achieving oleophobic behavior. Finally, three design profiles for three different wire diameters were proposed and one design profile was investigated for mechanical robustness. It can be concluded that even though oleophobic behavior can be achieved with the proposed designs, appropriate surface coating is necessary to achieve oleophobic behavior for element-pulley contact in CVT working conditions.

List of acronyms

CVT	Continuous variable transmission
DLC	Diamond like carbon coating
LST	Laser surface texturing
EDM	Electrical discharge machining
OWRK	Owens, Wendt, Rabel and Kaelble

Table of Contents

Chapter 1

Introduction

1.1 Motivation and framework

Ever since the continuous variable transmission CVT has been introduced in the global market its share has been increasing. Use of CVT equipped drivelines in the automotive industry have enabled customers to enjoy a fuel efficient, smooth and comfortable drive. According to press release by Bosch published in 2013 one in five automated transmissions was a CVT and the global share is expected to increase to 25 % by 2020 [1]. This success is mainly achieved with the reduction of the inner frictional losses over the last years. This report is also a continuation of the same effort and is aimed at improvement in wettability and frictional behavior of element-pulley and element-loop interface in the CVT push belt. This can be achieved by reduction of internal frictional losses between element-loop contact and increase of frictional forces in element pulley contact. Such a modification in the frictional forces would facilitate improvement in power density and efficiency of the CVT components.

The idea here is to alter internal frictional forces by altering the surface wettability of CVT components. A thorough investigation is required to connect internal frictional forces with the surface wettability. To address this problem research will be done at the advanced engineering department (ENA) of Bosch transmission technology Tilburg.

1.2 Goals of the assignment

The goals of the research are as follows:

- Determination of surface wettability of the CVT components (pulley, element, loop) with a number of CVT fluids
- Selection of the appropriate surface modification technique for obtaining the desired wettability behavior
- Define the optimal parameters of the selected technique

1.3 Outline

Chapter 2 explains the governing principle of surface wettability behavior. The key factors that define a specific wettability behavior and the forces responsible for those key factors are elaborated. In chapter 3 the experimental methods used to determine and quantify the surface wettability are presented and the results obtained from the performed experiments are stated. After presenting the results a hypothesis is proposed for correlation between surface wettability and frictional forces and subsequently element(flank) and pulley contact is chosen for surface modification. Different surface modification techniques for the stated contact and desired wetting behavior are examined in chapter 4. Furthermore, an appropriate surface modification technique is chosen and design parameters are optimized for oleophibic and mechanical robustness. Finally in chapter 5 conclusions and recommendations are drawn based on the proposed design and future areas of investigation are highlighted.

Chapter 2

Surface wettability

When a liquid encounters a solid surface, it can adapt one of the three behaviors, it can either completely wet the surface of the solid it encountered, it can adapt a shape of a droplet minimizing its contact area with the solid surface and the surface remains completely dry or it can partially wet the surface as shown in Figure 1[2].

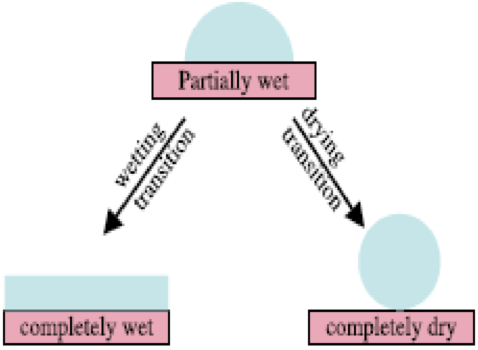

Figure 1 Three possible wetting states

Generally, surfaces are divided into two main categories based on their wetting behavior. This characterization is based on the contact angle formed when a certain liquid encounters a solid surface.

A contact angle is measured by producing a drop of liquid on a solid surface. The resultant angle formed between the solid/liquid interface and the liquid/vapor interface is referred to as the contact angle as shown in Figure 2 [3].

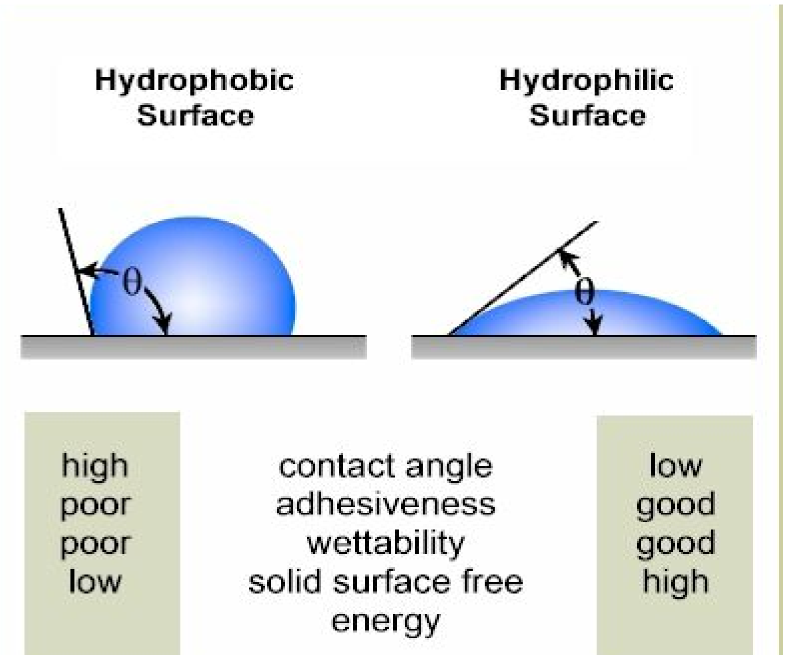

Figure 2 Types of contact angle measurements

If the contact angle is less than 90 degrees than the surface is said to be hydrophilic if the liquid is water and oleophilic if the interacting liquid is oil. Similarly, if the contact angle is larger than 90 degrees than the surface is said to hydrophobic if the liquid is water and oleophobic if the interacting liquid is oil. Furthermore, the terminology super hydrophobic or super oleophobic is used when the contact angle is larger than 150 degrees and super hydrophilic and super oleophilic is used when the contact angle is below 10 degrees.

The wetting behavior of a surface is governed by two main aspects that are the surface chemistry and surface texture. To understand the governing mechanism of these aspects an in-depth explanation of the governing mechanism is required. Section 2.1 explains in detail the governing principle of the role surface chemistry plays in defining the wettability behavior of a certain contact. Similarly, section 2.2 explains the role of surface geometry in defining the surface wettability behavior.

2.1 Role of surface chemistry in surface wetting behavior

Surfaces have long been modified in various fields to achieve desired surface properties like hardness, toughness and conductivity etc. Such surface properties can only be achieved if one understands the current physical and chemical state of the surface and is able to explain the surface chemistry from intramolecular and intermolecular point of view. When a liquid encounters the solid forces the intramolecular and intermolecular forces of solid surface start to attract liquid towards them. A brief introduction of the intermolecular and intra molecular forces that bonds atoms and molecules is as follows [4].

2.1.1 Intra molecular forces

The intramolecular forces present between atoms namely ionic bonds, covalent bonds and metallic bonds depend on the electronegativity of the atoms. In plain words electronegativity is the ability of an atom to attract shared electrons. Electronegativity increases and decrease in a certain pattern inside the periodic table. And the difference in electronegativity between two atoms defines the type of intramolecular bonding between those atoms.

2.1.1.1 Ionic bonding

There are different kind of interactions between different atoms that lead to several types of chemical bonds within these atoms. For example, a cation of sodium with positive charge will attract an anion of chlorine to form an ionic bond of sodium chloride molecule. As shown in Figure 3, chlorine gains one valence electron from sodium to fill its outer most orbit and a strong ionic bond is formed between sodium cation and chlorine anion.

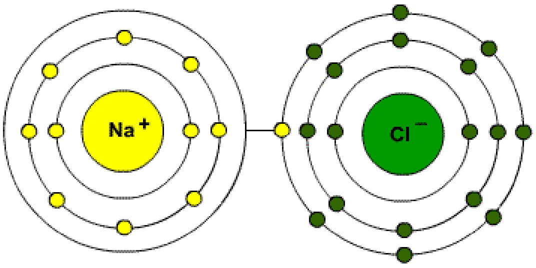

Figure 3 Ionic bond between sodium chloride molecule [4]

2.1.1.2 Covalent bonding

Similarly, a weaker attraction between different atoms will lead to covalent bonding where instead of electron transfer, electrons are shared between two atoms. For example, a water molecule is a result of electron sharing between the oxygen atom that needs two electrons to fill its outermost orbit and two hydrogen atoms that need one electron each to fill their outermost orbit as shown in Figure 4.

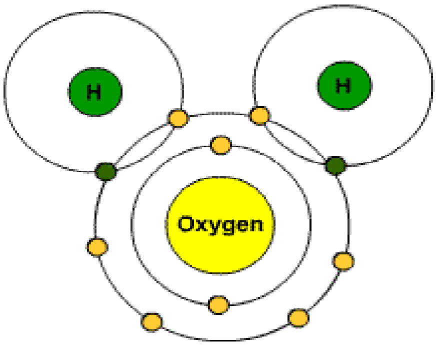

Figure 4 Covalent bonding in water molecule [4]

Covalent bonding can be further classified into two main classes namely polar covalent bonding and non-polar covalent bonding. The polarity of a certain covalent molecule depends on the electronegativity difference between the bonding atoms and the symmetricity of electron distribution.

Polar molecules are a result of non-equal electron sharing in a covalent bond. A dipole forms, with part of the molecule carrying a slight positive charge and the other part carrying a slight negative charge. This happens due to difference between the electronegativity of each atom. For polar molecules electronegativity difference ranges between 0.5 to 1.6. Another requirement for polar molecules is to have asymmetry between their electron distribution. Some of the examples of polar molecules are water - H_2O as shown in figure 3, ammonia - NH_3, sulfur dioxide - SO_2, hydrogen fluoride - HF and ethanol - C_2H_6O etc.

Nonpolar Molecules are a result of equal electrons sharing in a covalent bond. In this case there is no net electrical charge across the molecule and the electrons are evenly distributed. Generally, if the electronegativity difference between two atoms is less than 0.5 then the bond is considered nonpolar, even though the only truly nonpolar molecules are those formed with identical atoms. Some of the examples of non-polar molecules are noble gasses, diatomic elements like H_2, N_2, O_2 as shown in Figure 5.

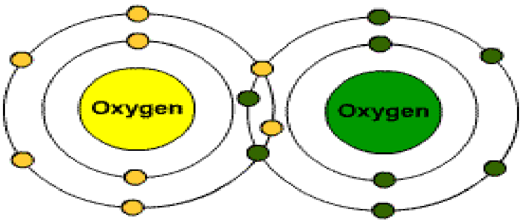

Figure 5 Non-polar covalent bond present in an oxygen molecule [4]

2.1.1.3 Metallic bonding

Similarly, metallic bonding arises from sharing of free electrons present in its structure among the positively charged cations. Since the outer shell of a metal is free to move, the electrons of the outer shell are released into an electron sea which is the structure of metallic bonding.

2.1.2 Intermolecular forces

Like attractions between atoms there are also attractions between molecules known as intermolecular forces. There are four main types of intermolecular forces namely Van der Waals forces, Dipole-dipole, hydrogen bonding and Ion-dipole. These intermolecular forces play a vital role as they hold the molecules together and play a role in defining the physical properties of the molecules.

2.1.2.1 Van der Waal forces

Van der Waals forces are the least strong intermolecular forces and are found in every molecule. They are a result of random movement of the electrons in a molecule that create temporary partial charge.

2.1.2.2 Dipole-dipole forces

Dipole-dipole forces are present between polar molecules, their strength increases with the electronegativity difference. They are a result of attraction between positive dipole of a molecule and negative dipole of another molecule and they are stronger when the dipoles have shorter lengths.

2.1.2.3 Hydrogen bonding

Hydrogen bonding is a special type of dipole-dipole force that is present between hydrogen and highly electronegative fluorine, oxygen or nitrogen and these intermolecular forces are stronger than both the Van der Waals forces and dipole-dipole forces.

2.1.2.4 Ion-dipole forces

Ion-dipole are the strongest type of intermolecular forces and are present between mixture of ionic compounds and polar compounds.

Figure 6 summarizes the type of intermolecular forces and displays their respective strength with comparison to other intermolecular forces.

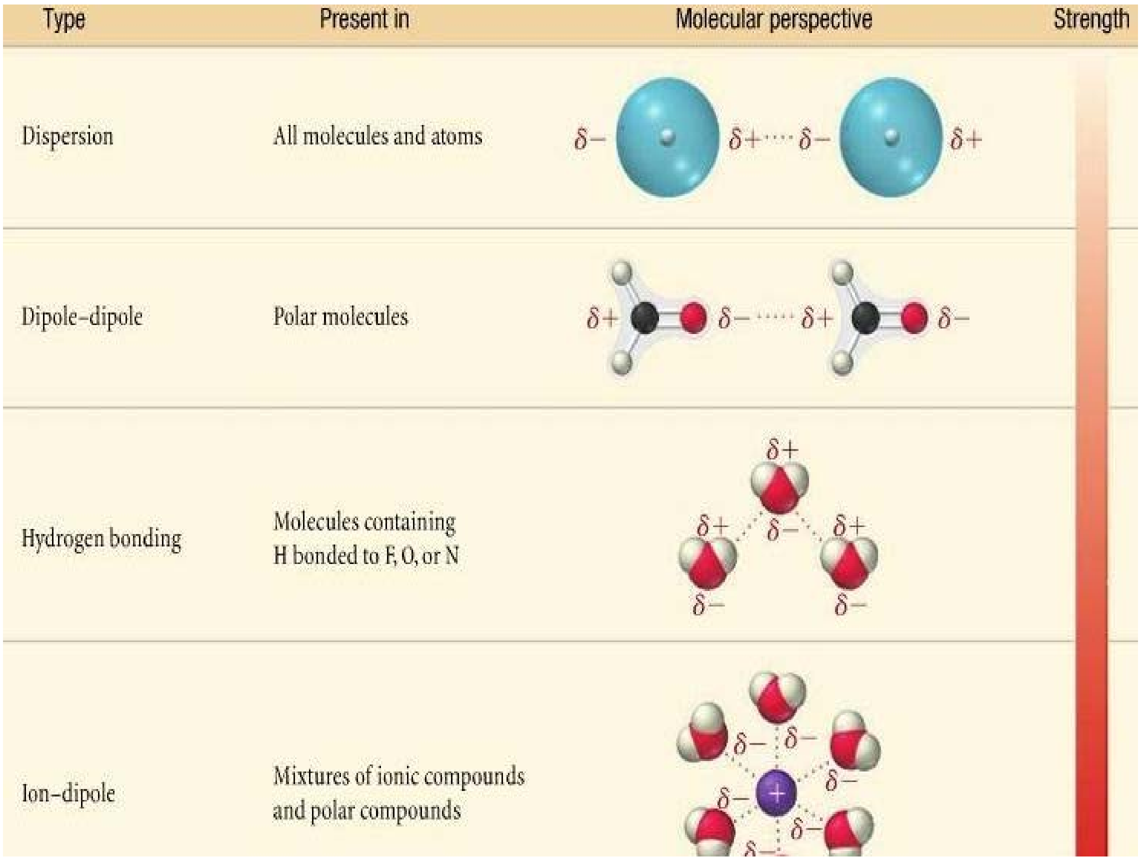

Type	Present in	Molecular perspective	Strength
Dispersion	All molecules and atoms		
Dipole–dipole	Polar molecules		
Hydrogen bonding	Molecules containing H bonded to F, O, or N		
Ion–dipole	Mixtures of ionic compounds and polar compounds		

Figure 6 Different intermolecular forces and their relative strength [5]

2.1.3 Governing mechanism

Depending on type and strength of intramolecular and intermolecular forces present of the liquid, the liquid spreads or forms a droplet. To have a perfect wetting the adhesive forces between the liquid and the solid must be significantly stronger than the cohesive forces of the liquid. Because in such a case the adhesive forces would enable maximization of the contact area between the solid and liquid surface. An increased contact area would facilitate more molecules to attract one another and therefore the liquid will spread better. Types of intramolecular and intermolecular forces with solid help characterize solid into two classes the so called high energy solids and low energy solids. The terminology is motivated from the term solid surface energy. In simple terms surface energy can be defined as follows.

> *"Surface free energy is the amount of work done per unit area to increase the size of the surface of a phase"*

Solids with stronger chemical bonds holding them together like ionic bonds and polar covalent bonds will require more energy to break them thus being high energy solids and solids with weaker chemical bonds holding them together like Van der Waals forces or hydrogen bonds will require comparatively less energy thus being the low energy solids. Role of surface chemistry in wetting behavior can be mathematically represented through the so-called Young's equation.

$$\sigma_{sg} = \sigma_{sl} + \sigma_{lg} \cdot \cos\theta \qquad (1)$$

In equation 1, θ represents the contact angle, σ_{lg} the surface tension of the liquid, σ_{sl} the interfacial tension between liquid and solid and σ_{sg} the surface free energy of the solid.

Another important aspect that can be concluded from young's equation is a better wetting can be achieved if the surface free energy of the solid σ_{sg} is greater than the surface tension of the liquid σ_{lg}.

Significance and role of polar and dispersive components of surface free energy in surface wetting behavior

Surface free energy of the materials is composed of polar and dispersive components and these components play a leading role in defining the wetting behavior of the surface. Since, there is no easy bonding between polar and non-polar molecules, identification of the polar and dispersive components of the surface energy for interacting phases is very important. Polar and dispersive components of surface energy are a result of different types of interactions between atoms and molecules meaning different type of intra and intermolecular forces present between atoms and molecules. Dispersive component is the result of temporary fluctuations of the charge distribution in the atoms/molecules of weak forces like Van der Waals forces. Similarly, polar component is a result of Coulomb interactions between permanent dipoles like the ones in ionic bonds and between permanent and induced dipoles like the ones present in hydrogen bonds [6]. As an example, two cases are presented in Figure 7, in the first case where the interacting phases possess equal polar and dispersive components good bonding between the two phases is evident. Similarly, in the second case bonding between the two phases is weaker due to dissimilar ratio of polar and dispersive components between the interacting phases [6]. Therefore, it can be concluded that similar ratio of polar and disperse components in the interacting phases is critical for improved wetting behavior.

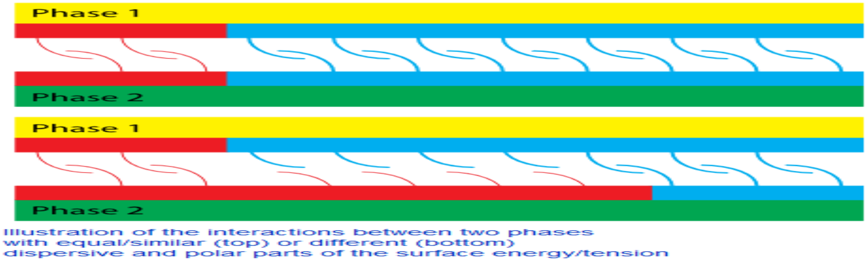

Figure 7 Interaction between two phases [6]

2.2 Role of surface geometry in surface wetting behavior

Surface geometry plays a critical role in defining the wetting behavior of a certain contact. Its role has recently gained a lot more importance since techniques like laser surface texturing, electrical discharge machining, laser and plasma etching have enabled easy creation of micro and Nano structures on material surfaces. Researchers have closely looked on the stunning examples of hydrophobic and oleophobic surfaces present in nature and tried to explain the role of surface geometry on their wetting behavior.

2.2.1 Wetting state of an oil droplet on a certain surface geometry

A liquid droplet can exist in one of the two wetting states on a certain surface geometry, the so called Wenzel state and Cassie-Baxter state. They are as follows.

2.2.1.1 Wenzel state

In this state the liquid droplet completely wets the surface it encounters and there are no air pockets trapped between the liquid droplet and the surface as shown in Figure 8.

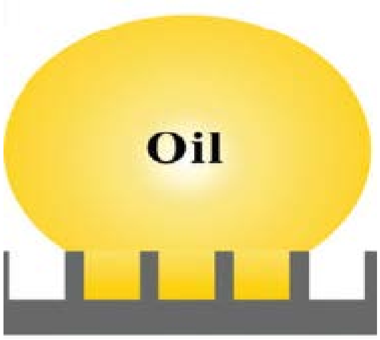

Figure 8 Wetting state of an oil droplet in Wenzel state [7]

Surface geometry like micro-dimples enable easy creation of Wenzel state with interacting liquids. In 1936 Wenzel studied the significance of surface roughness (0-10 microns) on a certain surface geometry and concluded that surface roughness will enhance the wetting behavior if the oil droplet is in Wenzel state [8]. So if the interacting surface is oleophilic by nature, creation of surface texture like micro-dimples on that surface and making it more rough will result in more oleophilicity. This phenomenon is mathematically explained in equation 2 that presented by Wenzel.

$$\cos\theta_m = \mathrm{r}\cos\theta_Y \tag{2}$$

In equation 2, θ_m represents the measured contact angle on a textured and rough surface, θ_Y the Young contact angle on a smooth surface and r is the roughness ratio.

The roughness ratio $r = \frac{\text{Actual solid surface area}}{\text{rojected solid surface area}}$. As no surface is perfectly smooth r >1 which implies from Equation 2 that for θ_Y< 90 → $\theta_m < \theta_Y$ and for θ_Y> 90 → $\theta_m > \theta_Y$ [9].

2.2.1.2 Cassie Baxter stage

In this state the liquid droplet wets part of the surface geometry it encounters, and the droplet sits partially on the surface and partially on top of the air pockets that are trapped between the liquid droplet and the surface as shown in Figure 9.

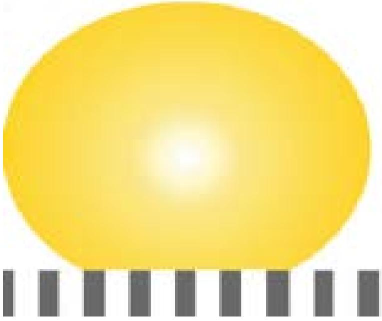

Figure 9 Wetting state of an oil droplet in Cassie-Baxter state [7]

Surface geometries like re-entrant surfaces are most commonly used to create robust Cassie-Baxter state between the interacting liquid and the solid surfaces [10]. Cassie and Baxter in 1944 studied the wetting state of liquid sitting partially on surface and partially on air pockets and concluded that measured contact angle θ_m,depends on the fraction of liquid in contact with the solid surface as presented in Equation 3 [11].

$$\cos\theta_m = x_1(\cos\theta_Y + 1) - 1 \tag{3}$$

In equation 3, x_1 represents the fraction of the surface that is in contact with the liquid. Since then many surface textures have been designed to achieve Cassie-Baxter state and increase the measured contact angle θ_m by altering the fraction of liquid in contact with the solid surface.

Different surface textures are designed to achieve Cassie-Baxter and consequently make surfaces more hydrophobic and oleophobic. Techniques like LST, chemical etching, plasma etching, electro discharge machining, lithography are used to construct the desired surface textures. Figure 10 displays a hydrophobic surface constructed by creating surface texture using LST technique [12].

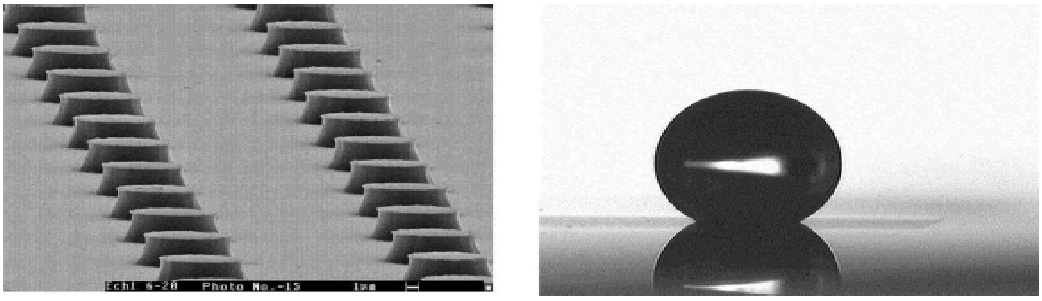

Figure 10 Super hydrophobicity by surface texturing. Left: patterned surface. Right: Water droplet on the textured surface

Surface roughness (0-10 microns) on surface geometries with surface textures (roughness > 10 microns) that support Cassie-Baxter stage can have both positive and negative impact on the wetting behavior. For instance, a carefully designed Nano-scale wavy structure on a microstructure wall surface texture can enhance the measured contact angle for a given contact. Similarly, undersigned roughness of few microns can result in reduction of measured contact angle in Cassie-Baxter stage.

2.3 Role of the lubricant in surface wetting behavior

Surface tension of the lubricant, wetting the surface as expressed in equation 1 is equally important and can significantly affect the wetting behavior. By altering surface tension of the liquid one can affect intra-molecular and inter molecular forces defining the wetting behavior of a certain engineering contact. Generally speaking, solids have stronger intramolecular and intermolecular forces than liquids. Thus, it has been observed that most liquids can easily wet high energy solid surface due to strong chemical bonds present in these solids. In case of low energy solid surface, the behavior of liquid depends on the force balance between surface energies of the interacting solid and liquid surface as explained in section 2.1.3. For the current research the CVT fluid, NS-3, is chosen and its properties like surface free energy and density will be used.

2.4 Chapter conclusion

In Chapter 2, basic introduction into the surface wettability and the governing mechanism of the wetting behavior are explained in detail. An insight has been provided into the role of surface chemistry of the surfaces, their surface geometry and the type of lubricant on the respective wetting behavior. It can be concluded that wetting behavior can be altered by modifying any of the above mentioned three categories.

Chapter 3

Surface wettability determination methods

3.1 Determination of surface energy for CVT solids

There are several methods that are used in practice to determine the surface free energy of solids e.g. OWRK method, van Oss method and Wu method. All these methods use contact angle measurements to determine the surface energy [13]. OWRK method is among the most common one which considers the geometric mean of the dispersive and polar components of the liquid's surface tension and of the solid's surface energy. The mathematical expression is presented in Equation 4 [13]. To determine the surface free energy of a solid surface using OWRK method, first contact angle measurements need to be performed for several model liquids on that solid surface. Model liquids are liquids whose polar and dispersive components are well known, among the most commonly used model liquids are diazomethane, ethylene glycol and thiodiglycol.

$$\sigma_{sl} = \sigma_s + \sigma_l - 2\sqrt{\sigma_s^D \sigma_l^D} - 2\sqrt{\sigma_s^P \sigma_l^P} \tag{4}$$

Substitution of Equation 4 into Equation 1 given linear equation of the type $y = mx + c$ can be as presented in Equation 5.

$$\frac{\sigma_l(1+\cos\theta)}{2\sqrt{\sigma_l^D}} = \sqrt{\sigma_s^P} \times \sqrt{\frac{\sigma_l^P}{\sigma_l^D}} + \sqrt{\sigma_s^D} \tag{5}$$

In Equation 5, y and x contain the known quantities, namely the measured contact angle, the dispersive and polar parts of the model liquid's surface tension. The desired dispersive and polar parts of the solid's surface energy are contained in the axis intercept c and in the slope m, respectively. These parameters are evaluated by creating a regression line and the desired solid's surface energy can thus be obtained. For better accuracy contact angles of at least three model liquids are preferred.

3.2 Determination of surface tension of the liquids

Similarly, there are several methods for the determination of surface tension of the liquids. Some of the well-known methods are capillary rise method, stalagmometer method – drop weight method, Wilhelm plate or ring method and maximum bulk pressure method. The surface tension of the liquid surface can be determined by using one of the above-mentioned methods.

3.2.1 Determination of overall Surface tension

The overall surface tension of the CVT lubricant, NS-3, was determined from pendant drop method [14]. Pendant drop is a well-known method where the image of the droplet hanging on the dosing needle is captured and the shape of the droplet, shown in figure 11, is analyzed using Young-Laplace equation presented as equation 6 where P_{int}represents the pressure inside the curved liquid surface, P_{ext} represents the pressure outside the curved liquid surface, R_1 and R_2 the radii of curvature and σ the surface tension of the liquid.

$$\Delta P = (P_{int} - P_{ext}) = \sigma\left(\frac{1}{R_1} + \frac{1}{R_2}\right) \tag{6}$$

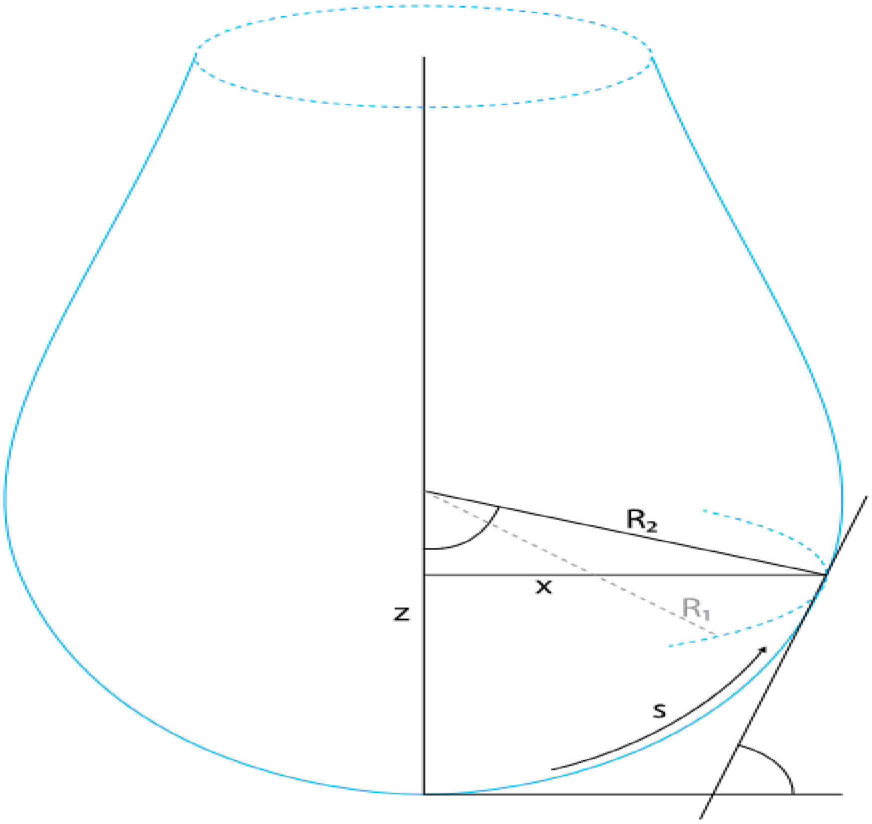

Figure 11 Derivation of Young-Laplace fit on the pendant drop [14]

The shape of the droplet owes its shape to two forces that are surface tension and gravitational force. Both forces effect the shape in opposite direction where the surface tension seeks to minimize the surface area and get the drop into a spherical shape. Gravitational force on the other hand stretches the drop from this spherical shape and the typical pear-like shape results as displayed in Figure 11.

By introducing the effect of gravity due to Pascal's law (hydrostatic pressure) setting reference at the vertex, which is the lowest point of the droplet and substituting $R_2 = x/sin\emptyset$, Equation 6 leads to Equation 7.

$$\frac{1}{R_1} + \frac{sin\emptyset}{x} = \frac{2}{R} \pm \frac{\Delta\rho g z}{\sigma} \tag{7}$$

Parametrization using the arc length s of the drop shape results into set of three first-order differential equations presented as Equation 8-10, with three boundary values, which can be solved by numerical procedures to determine the overall surface tension/ energy of the lubricant.

$$\frac{d\emptyset}{ds} = -\frac{\sin\emptyset}{x} + \frac{2}{R} \pm \frac{\Delta\rho g z}{\sigma} \quad (8)$$

$$\frac{dx}{ds} = \cos\emptyset \quad (9)$$

$$\frac{dz}{ds} = \sin\emptyset \quad (10)$$

3.2.2 Determination of the components of the Surface tension/energy

For determining the components of the surface tension, a method like the one used for determination of the surface energy of the solids can be used. But instead of using model liquids we will use a surface with zero or negligible polar component of surface energy in this case PTFE (Teflon) to determine the dispersive component of the surface tension using equation 11 [15].

$$\sigma_l^D = \left(\frac{{\sigma_l}^2}{72}\right)(\cos\vartheta_{PTFE} + 1)^2 \quad (11)$$

and the polar component of the surface tension/energy can then be determined by Fowke's method the mathematical expression of which is presented in Equation 12 [13].

$$\sigma = \sigma_P + \sigma_D \quad (12)$$

Experimental results of CVT components

3.3 Surface tension of the lubricant (NS-3)

The overall average surface tension of CVT fluid NS-3 determined from the method explained in section 3.2.1 is 37.37 mN/m. The average value was determined over 5 measurements. The calculated dispersive and polar component of the surface tension are 5.84 mN/m and 31.53 mN/m respectively determined from the method explained in section 3.2.2.

3.4 Surface energy of the CVT components

The contact angle measurements to determine the surface energy were performed on the following samples.

- Loop material after nitriding, measurements performed on the inner and the outer surface of the loop.

- Loop material before nitriding, measurements performed on the inner and the outer surface of the loop.
- End of line element samples
- End of line element samples- Flank profile
- Pulley surface sample

Before the measurements the samples were washed in an EMO machine for 10 minutes, cleaned with acetone and dried with warm air prior to measurements. Afterwards the samples were clamped on both sides to flatten the surface and to minimize the effect of curvature for loop samples. The liquids used for contact angle measurements were Demi-water, Ethylene glycol, Diazomethane and NS-3. Five droplets of each liquid were placed on the samples so that a mean value of contact angle per liquid per sample can be determined. Figure 12 presents the contact angle measurements for the samples.

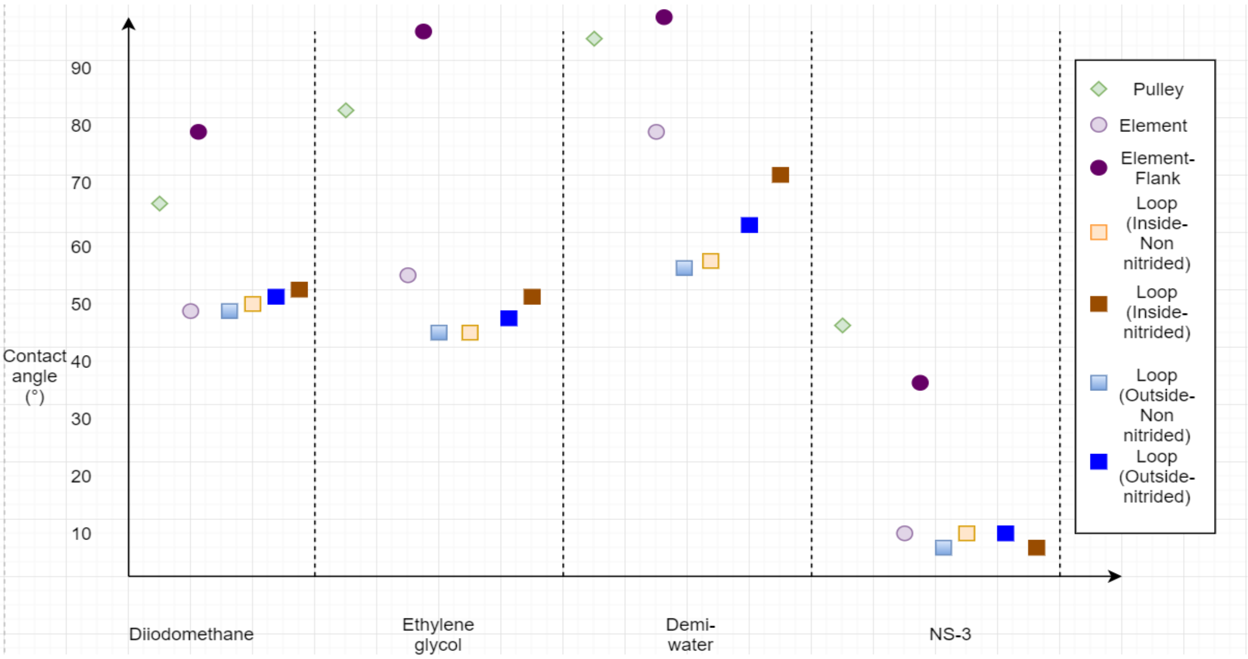

Figure 12 Contact angle values of the CVT components

Similarly, Figure 13 presents the calculated surface free energy and its polar and dispersive components through methods explained in section 3.2.2.

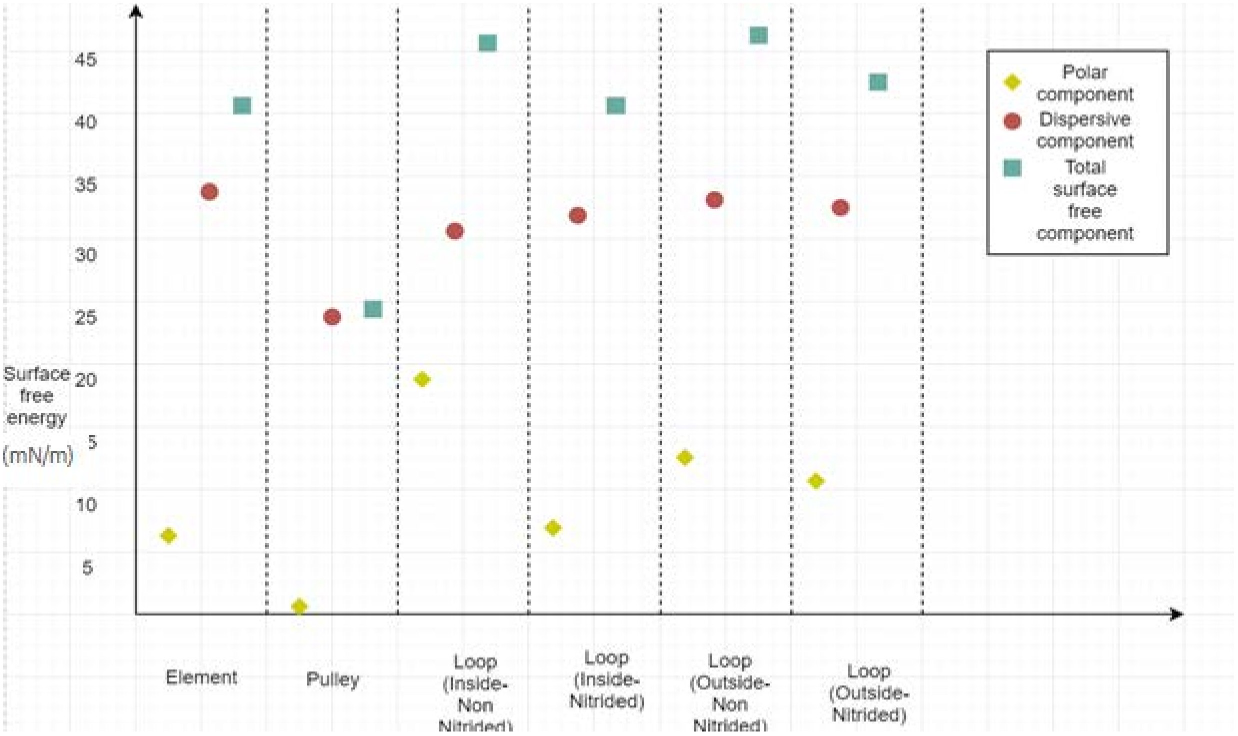

Figure 13 Calculated surface free energy and its components for the samples

3.5 Correlation between friction and wettability

As the contact angles measurements and surface tension/energy results reveal currently we have super oleophilic element(flank) and an oleophilic pulley surface. From Stribeck curve shown in Figure 14 [16], we know that for boundary, mixed and part of hydrodynamic lubrication regime the thicker the lubrication film is and lower is the coefficient of friction. Furthermore, literature has shown that the wetting performance benefits in building up the oil film that carries load and isolates surfaces. So from theoretical perspective the smaller the contact angle is the better is the lubrication [17].

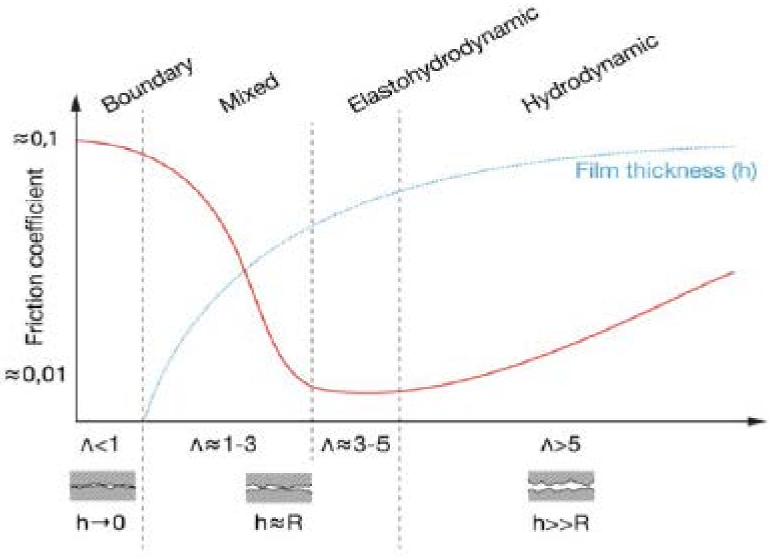

Figure 14 Stribeck curve and oil film thickness in a contact [16]

Therefore, the following hypothesis is proposed for the element(flank) – pulley contact.

> *"Presence of oleophobic surfaces in element(flank)-pulley contact would result in reduction of oil film thickness at the contact. Consequently, the current coefficient of friction would move to the left in Stribeck curve, resulting in an increase in the coefficient of friction at the contact. Such an improved coefficient of friction would enable improved power density and efficiency of the CVT Belt."*

3.6 Conclusions from the contact angle measurement results

Following conclusions can be drawn from the results of contact angle measurements.

- Element-Element contact: Very good wettability, super oleophilic wetting behavior.
- Element-Loop contact: Very good wettability, super oleophilic wetting behavior.
- Element (flank)-Pulley contact: Higher contact angle for NS-3 in comparison to other contact, oleophilic wetting behavior.

- **Roughness effect**: Based on the nature of roughness profile namely the Wenzel state or Cassie-Baxter state the roughness profile can affect the wetting behavior. Generally, for Wenzel state profiles the wetting behavior is further enhanced so an oleophilic surface will become even more oleophilic and an oleophobic surface will become even more oleophobic as explained in section 2.2.1.1. This effect can be seen when comparing the contact angles between loop inside and outside profiles. The Cassie-Baxter state enables to increase the contact angles as seen in case for element flank profile and as explained in section 2.2.1.2.
- **Lubricant effect:** Contact angle measurements vary significantly based on the type of the lubricant. The CVT fluid NS-3 has a low surface tension lubricant in comparison to other lubricants used for the experiments. Being low surface tension fluids and due to possessing higher dispersive component of surface tension oils generally show oleophilic behavior to steel surfaces.
- **Surface heat treatment effect:** Heat treatment techniques like nitriding modify the surface chemistry of the surface and leads to different wetting behavior in of the surface in comparison to untreated surface. The contact angle strongly depends on the surface chemistry and the interacting lubricant. For CVT loops the contact angle slightly increases when a nitride layer is applied on the surface.

It is known that element-loop contributes the most in the improvement of the desired frictional behavior but due to super oleophilic nature of the contact there is not much to gain in the given operating conditions. However, for element (flank)-pulley there is a potential for improvement as shown in Figure 12 and the desired oleophobic wetting behavior can be achieved by surface modification. Therefore, the aim of surface modification is to achieve oleophobic surfaces for element(flank)-pulley contact.

3.7 Chapter conclusion

In chapter 3, the surface energies of the CVT samples and CVT fluid, NS-3, were determined using contact angle measurements. It was found that element-element and loop-loop contact possessed super oleophilic behavior. In light of proposed hypothesis, the wetting behavior of these contacts is in accordance with the desired wetting behavior. However, it was observed that in case of element-pulley contact the desired wetting behavior can be achieved by applying appropriate modification technique and there is a room for improvement in the wetting behavior of this contact.

Chapter 4

Surface wettability modification techniques to achieve oleophobicity

The desired oleophobic behavior can be achieved by surface modification in two main directions.

- Changing the surface chemistry of surfaces
- Changing the surface geometry

Mostly combined approaches are used for achieving more robust oleophobic surfaces. As presented in Figure 15 a robust olephobic surface is a combination of the above mentioned two conditions and a re-entrant geometry.

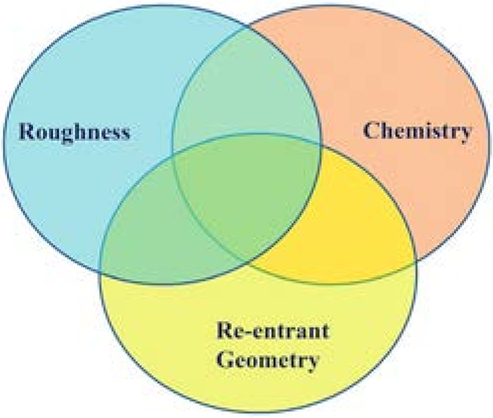

Figure 15 Basic design parameters for super oleophobicity [18]

4.1 Techniques used for surface chemistry modification

4.1.1 DLC Coatings

DLC Coatings are used substantially in engineering contacts mainly due to their high wear and abrasive resistance properties. A closer look at wetting behavior of several DLC coatings show improved contact angle value for fluorinated DLC coating in case of PAO oil as displayed in figure 16 [13,19].

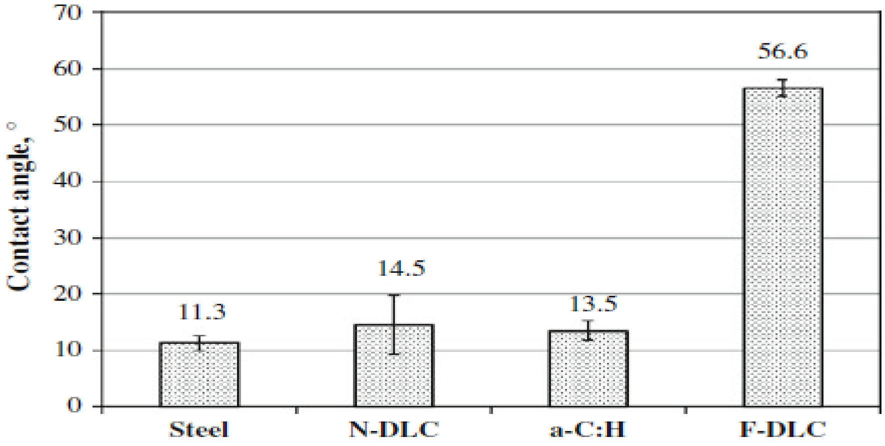

Figure 16 Contact angle values of PAO oil on steel, N-DLC, a-C:H and F-DLC coatings [19]

Similarly, Figure 17 displays that the high contact angle value for Fluorinated DLC is due to its decreased surface energy value in comparison to other DLC coatings. The lower the surface energy is a surface the higher the contact angle value it possesses for a given lubricant.

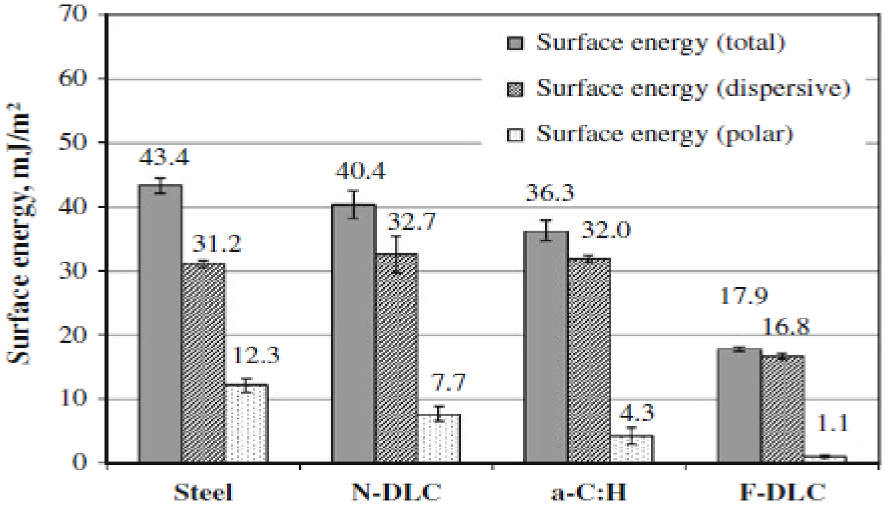

Figure 17 Surface energy values and corresponding dispersive and polar components of steel, N-DLC, a-C:H and F-DLC coatings [19]

Although Fluorinated DLC coatings has shown improved contact angle and promising results in the automotive industry by reducing wear in various engineering contacts [20-23]. Due to the change in the surface chemistry the co-efficient of friction reduces in the contact in comparison to steel-steel contact as shown in Figure 18, which is in contrast with the desired frictional behavior for the contact. Furthermore, the coefficient of friction is very low in comparison to the frictional values for element-pulley contact along with other operating conditions difference. Therefore, the only major remark is that use of DLC coatings in place of steel- steel contact results in lower coefficient of friction.

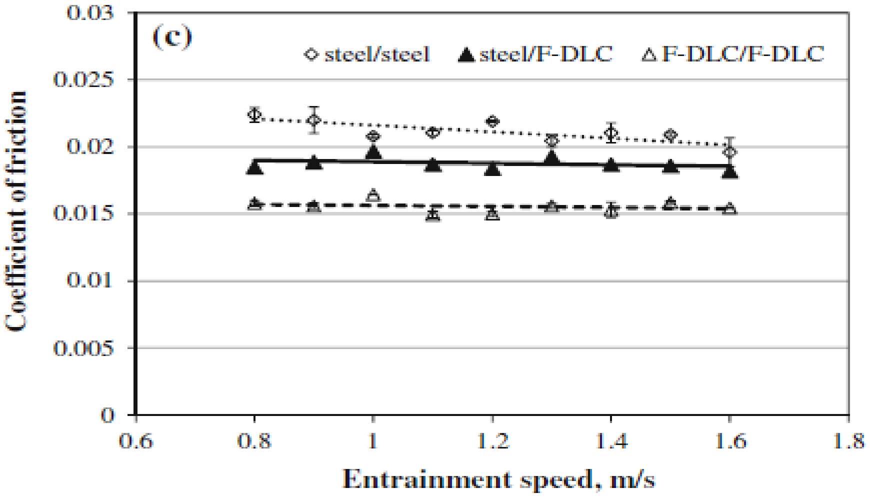

Figure 18 Coefficient of friction in PAO9 lubricated contacts for F-DLC coatings [19]

4.1.2 Plasma related surface chemistry modification techniques

Famously known as the fourth state of matter, and well known for its electric conductivity, a display of which can be seen in fluorescent tubes, plasma is being used in the industry for surface chemistry modification mainly for polymer surfaces [24]. There are two ways for plasma functionalization the so-called plasma activation and plasma polymerization. The latter is more reliable and durable as it enables polymerization of the surface with the desired functional group in an efficient manner. Some of the plasma motivated surface chemistry modification techniques are as follows.

4.1.2.1 Surface activation/passivation

Plasma is used to increase or decrease the surface energy of the surface. This enhances the adhesion properties of the surface resulting in improved wetting behavior.

4.1.2.2 Plasma enhanced chemical vapor deposition (PECVD)

Several coatings can be applied on plasma activated surfaces. Among main coatings that are applied are SiO_2 and PTFE coatings. Coatings with desired chemistry like NH_2, hydroxyl group and epoxide groups can also be deposited on the surface using plasma technology. To achieve the desired oleophobic behavior fluorinated plasma coated surfaces can be constructed using plasma technology.

4.2 Techniques used for surface geometry modification

Inspired by nature and astonished by wetting behavior of lotus leaf, spider web and other species many researchers were motivated to investigate the wetting behavior of these example and model the same wetting behavior to be used for various applications. Studies have shown that super hydrophobic behavior of surfaces possess their behavior due to the presence of Nano and microstructures on the surface [20]. In situations where liquid does not penetrate the grooves the so called Cassie-Baxter stage is formed resulting in oleophobic behavior of surfaces. As already stated in section 2.2 surface geometry plays a key role in defining the surface wetting behavior of a surface and techniques like LST and EDM most commonly used to construct the desired surface geometry on the solid's surfaces [25-27].

4.2.1 Significance of re-entrant microstructures

The micro-structure of the material surfaces can be roughly divided in to two types: trapezoidal and inverted trapezoidal shown in Figure 19 (a&c) and (b&d) respectively. With θ being the Young's contact angle and ψ being the local geometric angle of the texture. For $\theta < \psi$ there is downward net traction in liquid air interface due to capillary force, which promotes diffusion of lubricant and increases in volume of the lubricant into the solid texture as shown in Figure 19a consequently leading to a fully wetted state. However, for $\theta > \psi$ the net traction is upward, ensuring the robust Cassie-Baxer state as shown in Figure 19 (b, c and d) [7], [30]. Inverted-trapezoid surfaces shown in Figure 19 (b&d) also known as re-entrant textures have proven to be more reliable microstructure for achieving a robust Cassie-Baxter stage and have been regarded as the key parameter for achieving oleophobicity as shown in Figure 15.

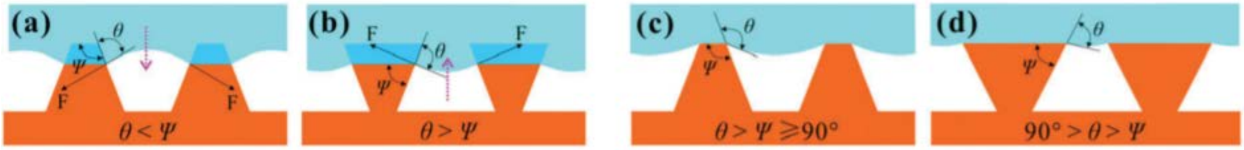

Figure 19 Different wetting behavior of a droplet on a surface on micro structure level

Many examples of super oleophobic surfaces with different surface geometry as shown in Figure 20 are available in the literature but mechanical robustness is questionable. Microstructures such as overhangs, rough metal meshes (e), micro pillars (g), micro inverted trapezoidal (h), Nano-nails (j) electro-spun fibers (f) and porous structures (a, b & c) have been used to achieve oleophobic behavior as shown in Figure 20 [7].

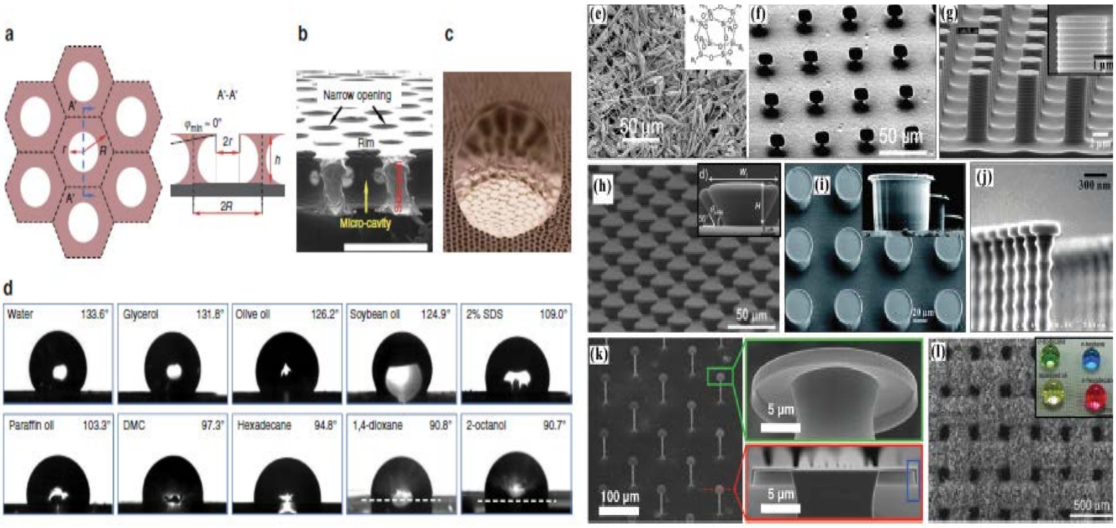

Figure 20 Various super-oleophobic surface created by re-entrant micro-textures.

4.2.2 Working mechanism of re-entrant surfaces

As described earlier the re-entrant surfaces with local texture angle ψ< θ facilitate the net traction of the liquid vapor interface to be upward, thereby supporting the formation of a Cassie-Baxter stage. This implies that a surface can support a composite interface (high contact angles and low roll of angles) if ψ< θ or it can get fully wet is ψ> θ.

Nosonvsky et al. analyzed the stability of composite interfaces on re-entrant surfaces and argued that to create stable composite interface one needs a local region where the texture angle (ψ) in the microstructure is equal to the equilibrium contact angle θ [29].

Furthermore, A. Tuteja et al studied the significance of reentrant curvature in the formation of a metastable composite interface [31]. They analyzed the variation in Gibbs free energy arising from the progressive penetration of the liquid air interface into various textured surfaces. Depending on the contact chemistry Gibbs free energy showed local minima for both composite interface and fully wetted state at different penetration depths. It was also concluded that re-entrant profile should be carefully design to prevent the transition from Cassie-Baxter state to fully wetted state under applied loading conditions.

4.2.3 Design parameters for robust oleophobic textures

Two dimensionless design parameters have been presented for oleo phobic robustness of the reentrant surfaces with micro-hoodoo profile (shown in Figure 20-f). The first one so called spacing ratio is calculated as $D^* = \frac{1}{x_1}$. The spacing ratio correlates measured apparent contact angle with the surface texture parameters. The Cassie-Baxter equation 3 can be rewritten in terms of spacing ratio and is presented in equation 13.

$$\cos\theta^* = -1 + \frac{1}{D^*}[\sin\theta + (180-\theta)\cos\theta] \qquad (13)$$

Thus, the higher the D* will be the higher the value of θ^* which is the apparent contact angle.

The second design parameter H* is presented to provide a realistic prediction of the breakthrough pressure. The robustness parameter H* quantifies the sagging of liquid vapor interface because of pressure difference across the interface. This pressure difference can result from various sources such as external pressure, impact of liquid droplet released from height and the Laplace pressure within the droplet.

The robustness parameter is calculated as $H^* = \frac{h_2}{h_1} = \frac{2[1-\cos\theta)R+(H-T)]l_{cap}}{(\frac{W}{2})^2}$, where h_1 is the sagging height of the droplet and h_2 is the original clearance between the liquid vapor interface and the next level of fibers as shown in figure 21. High values of H* indicate formation for robust Cassie-Baxter state under the assumed pressure conditions.

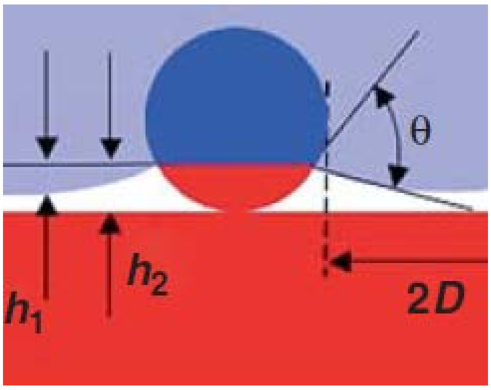

Figure 21 Lubricant behavior on an electro spun fiber

There are several techniques that can be used to create re-entrant textures. Some of the techniques are as follows. Among the most commonly used techniques for surfaces texturing are Laser surface texturing (LST), Plasma surface etching, Plasma surface grafting, Lithography and Electrical Discharge Machining (EDM)

4.3 Proposed technique

The decision for choosing the appropriate technique for further investigation on the CVT components was based on several aspects like feasibility of the technique for the material of CVT components, the oleophobic and mechanical robustness of the technique. It has been cited in the literature that most super oleophobic surfaces have poor mechanical durability, so their super-liquid repellent is easily lost after physical rubbing strong acid/alkali corrosion and so on

[7], [28]. Lately a lot of researches are focusing in improving the robustness and durability of these surfaces [18]. But as explained earlier the mechanical robustness of most of the olephobic surfaces prepared from various techniques is still an evolving field and thus any proposed technique will have to be experimentally tested for mechanical robustness and optimized for CVT working conditions afterwards.

The proposed technique is a step wise approach. In the first step construction of micro-mushroom re-entrant structures through micro electrical discharge machining method is proposed as shown in figure 22. The surface geometry is inspired by a study done by Patricia B Welsensee et al where they constructed hydrophobic and oleophobic steel surfaces by constructing micro-mushroom re-entrant textures on the steel surface and afterwards coating the surface with Teflon layer [28].

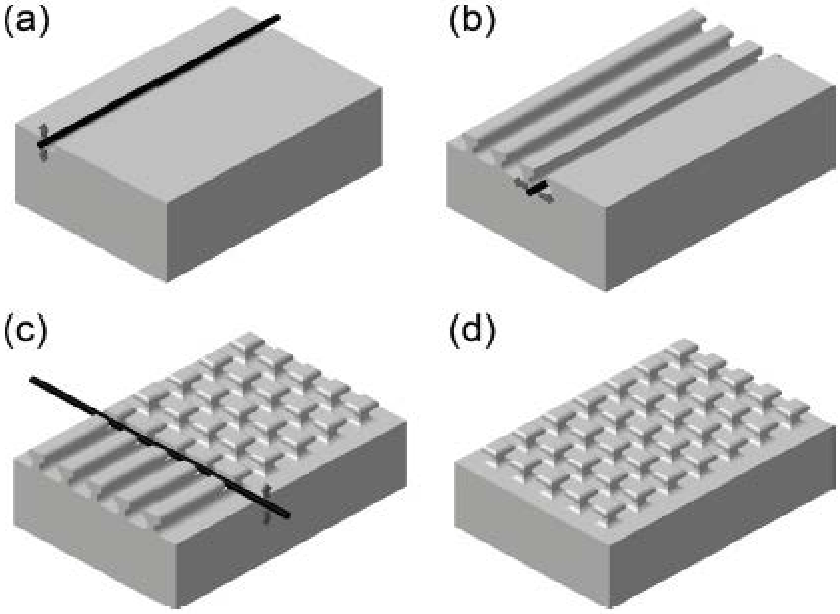

Figure 22 Micro-mushrooms fabricated on the steel surface [28]

Figure 23 shows the high contact angle that were achieved using the stated combined approach. This indicates that a combined approach of surface geometry and surface coating on the steel surfaces can help achieve super oleophobic behavior.

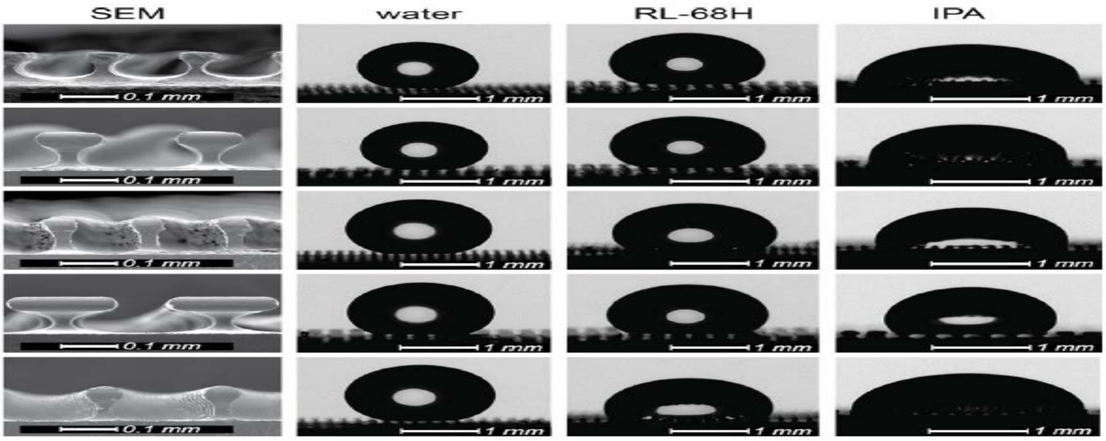

Figure 23 Hydrophobic and oleophobic steel surface roughness texture and contact angles [28]

The design parameters as shown in Figure 24 for the mushrooms (micro-hoodoo geometry) need to be optimized taking into consideration the following points. These points are summarized in light of the recommendation proposed by Anish Tuteja et al. in their study on super oleophobic surfaces for micro hoodoo geometry [29-30].

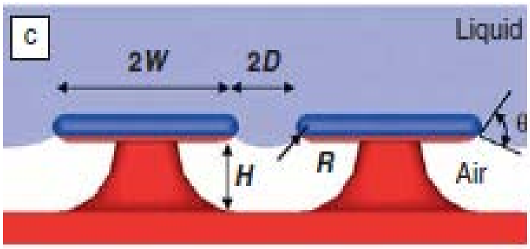

Figure 24 Design parameters of the mushrooms

1. Presence of a strong curvature implying R to be as small as possible.
2. Gap width ‘2D’ in accordance with the market supplier wire diameter limitations. From design perspective smaller values of D are preferred.
3. Mushroom head length ‘2W’ should be chosen in such a way to have a Mushroom head length to Gap width ratio larger than unity.
4. Optimization of the spacing ratio parameter D* and robustness parameter H*.

4.4 Design parameters optimization

The dimensions represented in Figure 25 were optimized taking into consideration the points mentioned in section 4.3.

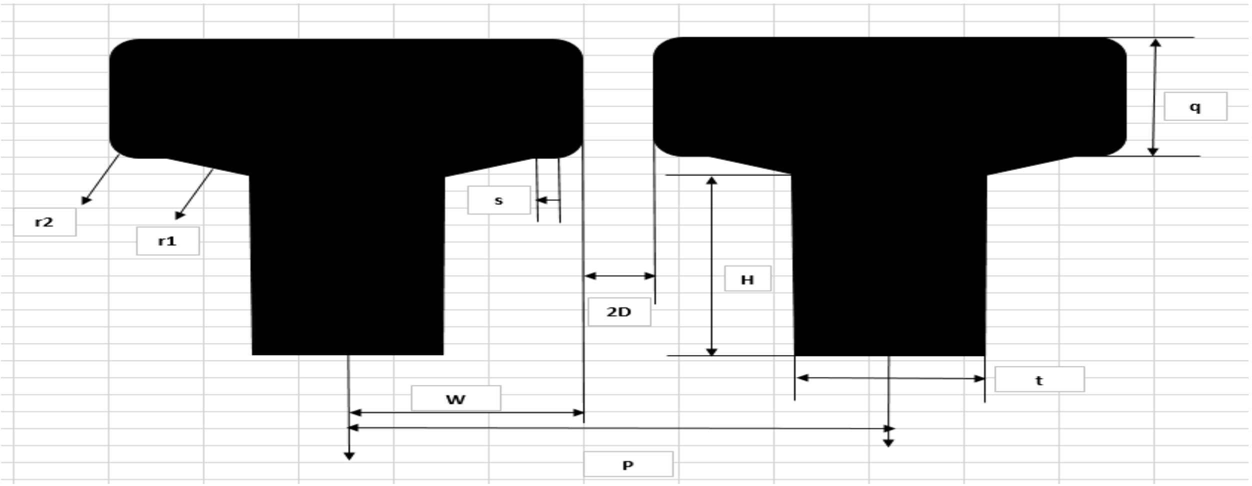

Figure 25 Dimensions of the constructed profile

A closer look into breakthrough pressure which is the critical pressure when liquid droplet transitions from Cassie-Baxter stage to fully wetted stage for T-shape pillar array surface shows that for a given D* the smaller the pillar diameter the higher the breakthrough pressure against wettability as shown in Figure 26 [18].

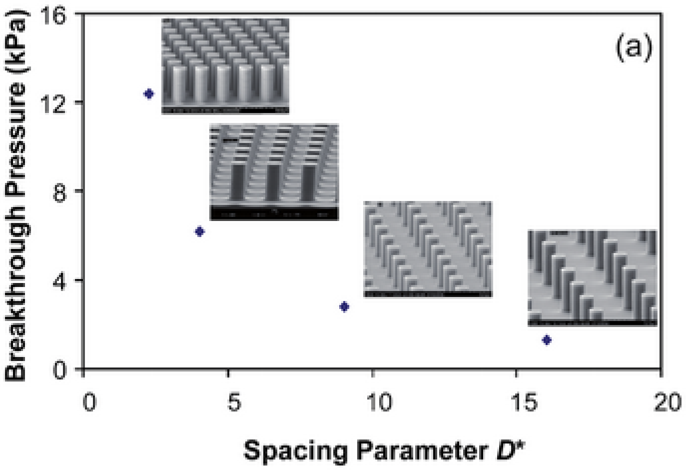

Figure 26 Plot pf breakthrough pressure as a function of D for T-shape pillar array surface [18]*

Therefore, a compromise need to be made between mechanical robustness and robustness against wettability. To analyze the change of robustness parameter H* and D* based on changing dimension ‘D’ and ‘H’ surface plots for three lubricants were plotted using MATLAB. Figure 27 represents the stated surface plots for NS-3. The surface plots for ethylene glycol and demi-water are presented in the Appendix.

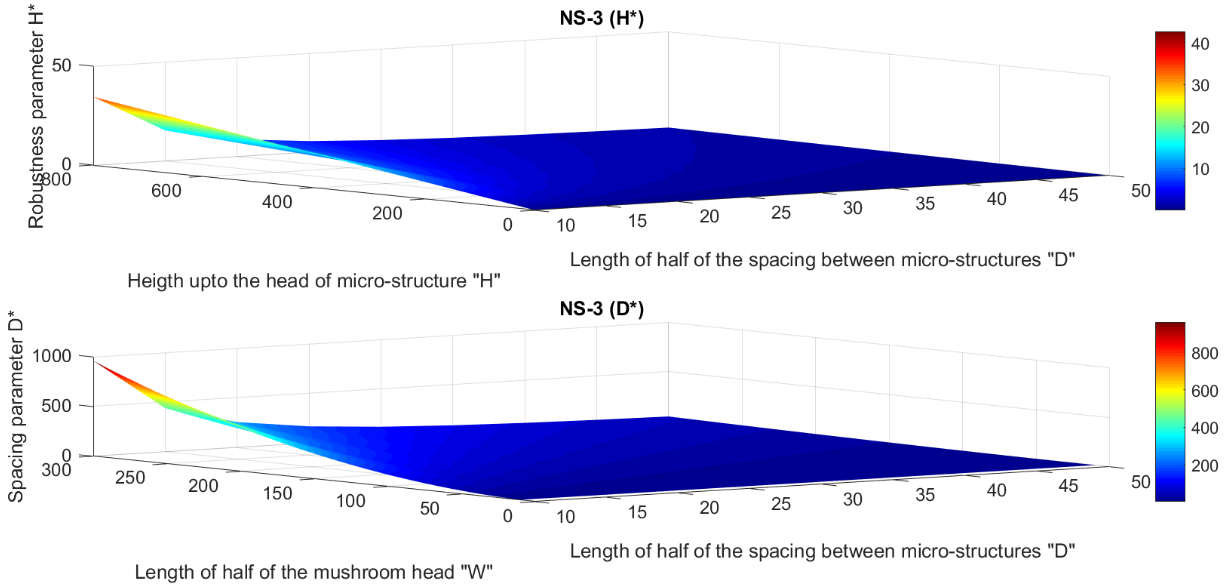

Figure 27 Surface plots representing dimensionless parameters H and D* for NS-3*

Similarly, the surface plot of apparent contact angle $\theta^*$for NS-3 presented in section 4.2.3 is shown in Figure 28. The surface plots of $\theta^*$for ethylene glycol and demi-water are presented in the Appendix.

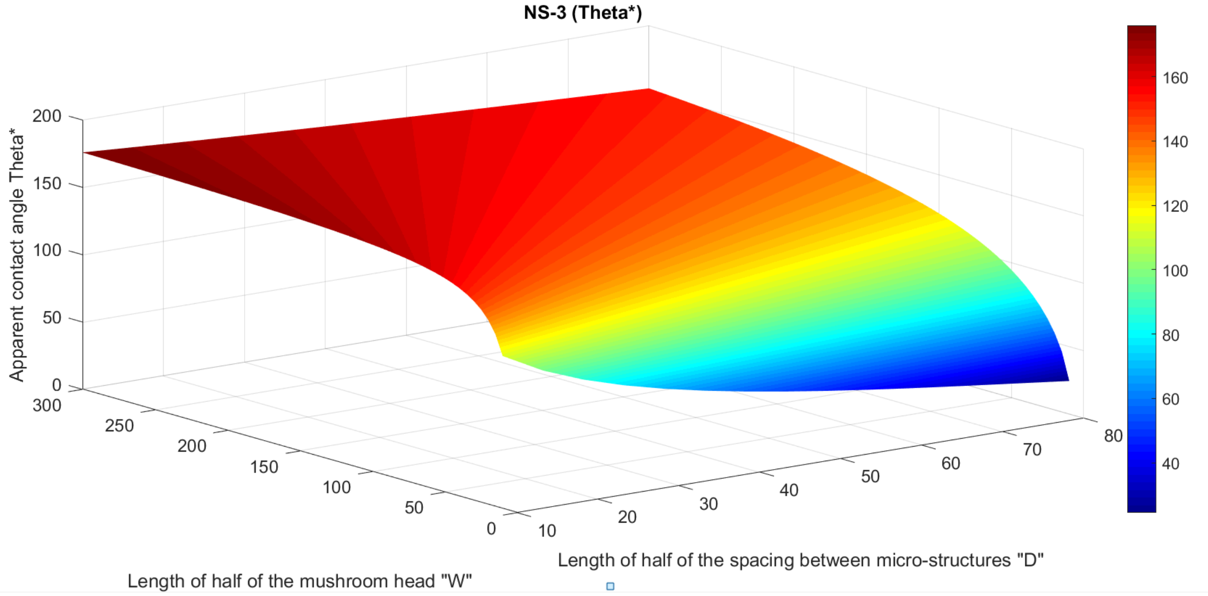

Figure 28 Surface plot of apparent contact angle for NS-3 in degrees

Based on the surface plots following observations can be made.

1. Lower spacing ‘D’ between the mushrooms provides higher values of H*, D* and $\theta^*$for all the three tested liquids.
2. Robustness parameter H* is inversely proportional to the square of parameter ‘D’. This shows that H* possess high values for lower values of the parameter ‘D’. As the parameter ‘D’ increases, H* values decreases.
3. A closer look at the color bar of H* shows that the important effect of lubricant on the values of H*. To achieve a composite interface for oleophobicity (high contact angles and low roll off angles), the value of H* should be higher than 1. For example, it is possible to achieve a H* value greater than 1 for Demi-water with higher values of D and lower value of H which is more challenging when using NS-3.
4. The higher the D* will be the higher the value of θ^*.

As described earlier through Figure 26 a trade-off has to be made between breakthrough pressure for robustness against wettability and mechanical robustness such that the structure can withstand the applied loading. For this reason, a relationship between design parameters ‘W’ and ‘D’ was addressed from mechanical robustness point of view. Mathematical expression for design parameter ‘W’ can be easily deduced from Figure 25 and is presented in Equation 14.

$$W = \frac{t}{2} + R_1 + s + R_2 \tag{14}$$

For analyzing the mechanical stability of the proposed design modelling of the proposed design was done, where some of the dimensions like D, R_1 presented in Table 1 were chosen in accordance with the manufacturers limitations. Other like H, Q, S and R_1 were chosen by optimizing the robustness parameter H*. As it is intended to perform frictional tests on the modified samples in the future using pin on disk frictional tests. The relationship between W and t is optimized in accordance with the applied loading and the pin dimensions. A rough estimation for the required area needed to satisfy the applied loading without exceeding the yield strength of the material is presented as inequality in Equation 15.

$$A_{support} \geq \frac{3}{16} \times A_{apparent} \tag{15}$$

Solving for equality where $A_{support} = t * t$ and $A_{apparent} = (W + 2D + W)^2$ and inserting value of W into Equation 14 leads to a quadratic Equation 16.

$$\frac{13}{16} * t^2 - \frac{3(R_1 + s + R_2 + D)}{4} * t - \frac{3}{4}\left((R_1 + s + R_2)^2 + D^2 + 2(R_1 + s + R_2)(D)\right) = 0 \tag{16}$$

A MATLAB code was written to determine required dimensions of W and t while modifying D, R_1, R_2 and S in accordance with supplier's limitation.
And the design dimensions for the created two geometries are presented in Table 1.

Wire Diameter (µm)	Size of unit P (±2) (µm)	Base width t (±2) (µm)	R_1 (±2) (µm)	R_2 (±2) (µm)	S (±2) (µm)	Q (±2) (µm)	H (±2) (µm)	W (±2) (µm)	D (±2) (µm)	H*	D*
70	390	170	45	10	10	100	600	150	45	1.28	18.8
50	320	140	35	10	10	100	360	125	35	1.27	20.89
30	250	105	25	10	10	100	190	100	25	1.33	25

Table 1 Proposed Design Dimensions of the Mushrooms

4.5 Mechanical robustness

The mechanical robustness of the proposed design for the manufacturing diameter of 70 microns was analyzed by designing a 3D model and applying loadings on a single mushroom. The mushroom's mechanical strength was investigated based on the applied loading as shown in Figure 29.

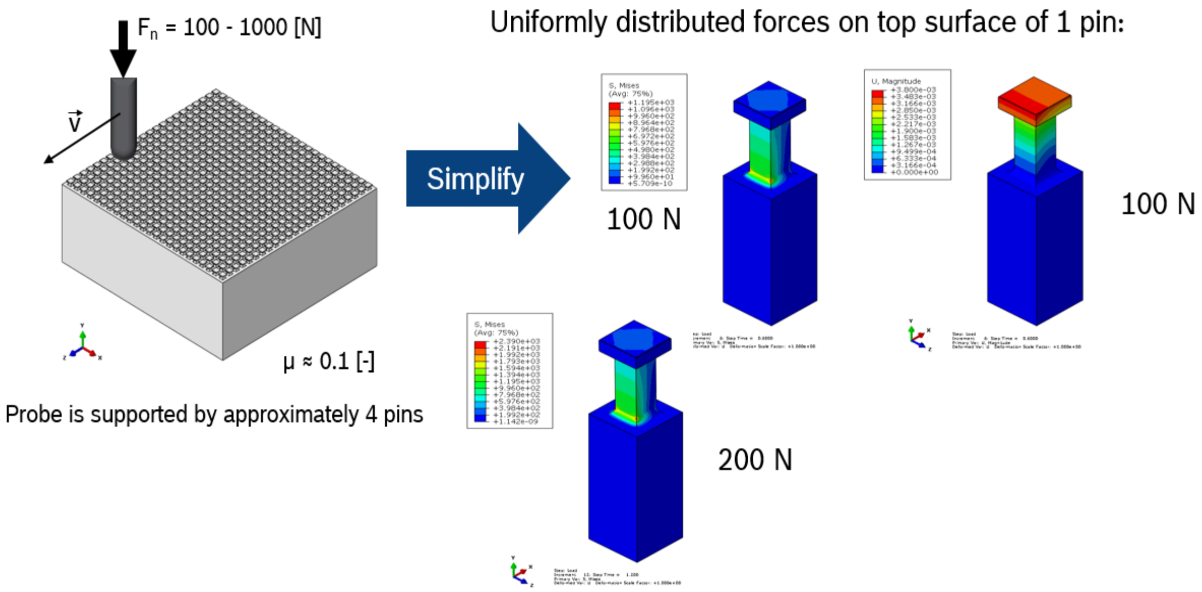

Figure 29 Mechanical robustness of a single mushroom

The mushroom can sustain an applied load of 100 N with a displacement of few microns but if the applied loading is increased to 200 N the localized stresses in the mushrooms exceed the yield stress of the material. Since the applied loading is much higher for element-pulley contact the presented design parameters must be optimized for mechanical robustness.

4.6 Chapter conclusion

In chapter 4 different surface modifications techniques were presented. A surface geometry modification that stated construction of micro-mushrooms reentrant surface geometry on the pulley surface was proposed. The 3D model of proposed design for 70 microns was designed and tested for mechanical robustness. It was observed that the current design parameters can hold up to 100 N of normal load and breakthrough pressure of up to 4Kpa. The desired normal load and breakthrough pressure for element-pulley contact is much higher than the current values and the design parameters should be optimized to achieve super oleophobic behavior in the element-pulley working conditions.

Chapter 5

Conclusions and recommendations

The report addressed the topic of surface wettability and aims to provide insight into the governing principle of the wetting behavior. The wetting behavior of element-element and pulley-pulley contact showed super oleophilic behavior. This wetting behavior is concluded to be quite good and in accordance with the desired wetting behavior for these contacts.

A room of improvement was observed for element-pulley contact and various surface modification techniques were explored to achieve the desired oleophobic behavior in this contact. A surface geometry modification by constructing micro-mushroom reentrant surface geometry was proposed and further investigated for oleophobic and mechanical robustness.

It can be concluded that with current design parameters the proposed design profile for 70 microns wire can sustain a normal mechanical load of 100N with a breakthrough pressure of up to 4kpa. These numbers are much lower than the required mechanical load and breakthrough pressure for element-pulley contact.

Therefore, to achieve the desired oleophobic behavior appropriate surface coating must be applied on top of the design profile and the design parameters must be optimized for mechanical robustness. Furthermore, experimental validation of the proposed hypothesis should be investigated by performing pin on disk frictional tests on the samples. This would facilitate in the validation of the proposed hypothesis presented in section 3.5 and analyze the wear and fatigue properties of the modified samples.

Bibliography

[1] *Bosch, "Continuously variable transmissions on the rise worldwide", Press Release: PI 8264 GS FF/Moe, 2013.*

[2] *Shashank Sarbada, Tung C. Shin, "Super hydrophobic contoured surfaces created on metal and polymer using femtosecond laser", February 2017.*

[3] *Rame-hart information on contact angle, Link: http://www.ramehart.com/contactangle.htm*

[4] *Ron Kurtus, "Types of chemical bonding", September 2015, Link: http://www.school-for-champions.com/chemistry/bonding_types.htm#.WgFmdEWfRAA*

[5] Image courtesy of (CHEM 210) chap. 11- Liquids, Solids, and Intermolecular Forces Flashcards) Link: http://www.cram.com/flashcards/chem-210-chap-11-liquids-solids-and-intermolecular-forces-978784.

[6] *Data physics, "Dispersive and polar parts of the surface energy/tension", Link: http://www.dataphysics.de/2/start/understanding-interfaces/basics/dispersive-and-polar-parts-of-the-surface-energytension/*

[7] Jiale Yong et al, "Superoleophobic surfaces", Chem.Soc. Rev.,2017,46,4168.

[8] *R.N. Wenzel, "Resistance of solid surfaces to wetting by water", Industrial and engineering chemistry 28 (1936) 988*

[9] *A. Marmur, "Soft contact: Measurement and interpretation of contact angles". Soft Matter 2 (2006) 12*

[10] *A. Tuteja et al., "Designing superoleophobic surfaces", Science 318 (2007) 1618.*

[11] *A.B.D. Cassie and S. Baxter, "Wettability of porous surfaces", Transactions of the Faraday Society 40 (1944) 546.*

[12] *Daniel Bonn, "Wetting and spreading", Reviews of modern physics, Volume 81, June 2009.*

[13] *M.Kalin, M. Polajnar, "The wetting of steel, DLC coatings, ceramics and polymers with oils and water: The importance and correlations of surface energy, surface tension, contact angle and spreading", December 2013.*

[14] *Data physics, "Pendant drop method — Optical determination of the surface/interfacial tension", Link: http://www.dataphysics.de/2/start/understanding-interfaces/drop-shape-analysis/pendant-drop-method/.*

[15] Link:https://www.kruss.de/fileadmin/user_upload/website/literature/kruss-ar213-en.pdf

[16] David Goncalves et al, “Film thickness and friction relationship in grease lubricated rough contacts”, August 2017.

[17] Linguo Qin et al., “Influence of surface wettability on the tribological properties of laser textured Co-Cr-Mo alloy in aqueous bovine serum albumin solution”, December 2012

[18] *Robin Ras et al., Non-wettable Surfaces : Theory, Preparation and Applications, Chapter 6.*

[19] *M.Kalin, M. Polajnar, “The effect of wetting and surface energy on the friction and slip in oil lubricated contacts”, September 2013.*

[20] *Kano et al., “DLC Coating technology applied to sliding parts of automotive engine. New Diam.Front. Carbon Technol.”, 2006, 16(4), 201-210.*

[21] *Neville et al., “Compatibility between tribological surfaces and lubricant additives-how friction and wear reduction can be controlled by surface/lube synergies. Tribol.Int.”, 2007, 40(10312 SPEC.ISS.), 1680-1695.*

[22] *Gahlin et al., “ME-C:H coatings in motor vehicles. Wear”, 2001, 249(3-4),302-309.*

[23] *Lin Feng et al., “Super-Hydrophobic Surfaces: From Natural to Artificial”, December 2002.*

[24] *Demetrius Chrysostomou, Director of Technology, PVA TePla America presentation, link: https://www.youtube.com/watch?v=5ejOYw8_3PU.*

[25] *Etison I., “State of the art in laser surface texturing”, Journal of Tribology, Vol 127, 2005, pp.248-253.*

[26] *Pettersson U. et l, “Influence of surface texture on boundary lubricated sliding contacts”, Tribology International 36, pp.857-864, 2003.*

[27] *Etison I., “Improved tribological performance of mechanical components by laser surface texturing”, Tribological Letters, Vol 17, No.4, 2004.*

[28] Patricia B Welsensee et al., “Hydrophobic and oleo phobic re-entrant steel microstructures fabricated using micro electrical discharge machining”, August 2014.

[29] Anish Tuteja et al, “Design parameters for super hydrophobicity and superoleophobicity”, August 2008.

[30] Arun K. Kota et al, “Super oleo phobic surfaces: design criteria and recent studies”, February 2013.

[31] A. Tuteja, W. Choi et al, Science 318(5856)1618 (2007).

Appendix

Average contact angles of end of line element sample

Average contact angles of four described lubricants on two end of line element samples are presented in Table A. Furthermore, the screen shots of the contact angle for Demi-water and NS-3 are displayed in Figure A.

Sample	**Average contact angle value over five measurements CA [°]**			
	Diazomethane	**Ethylene glycol**	**Demi-water**	**NS-3**
Element sample 1	46.26	52.57	70.05	8.65
Element sample 2	47.40	55.20	86.85	-

Table A Contact angle measurements of the samples

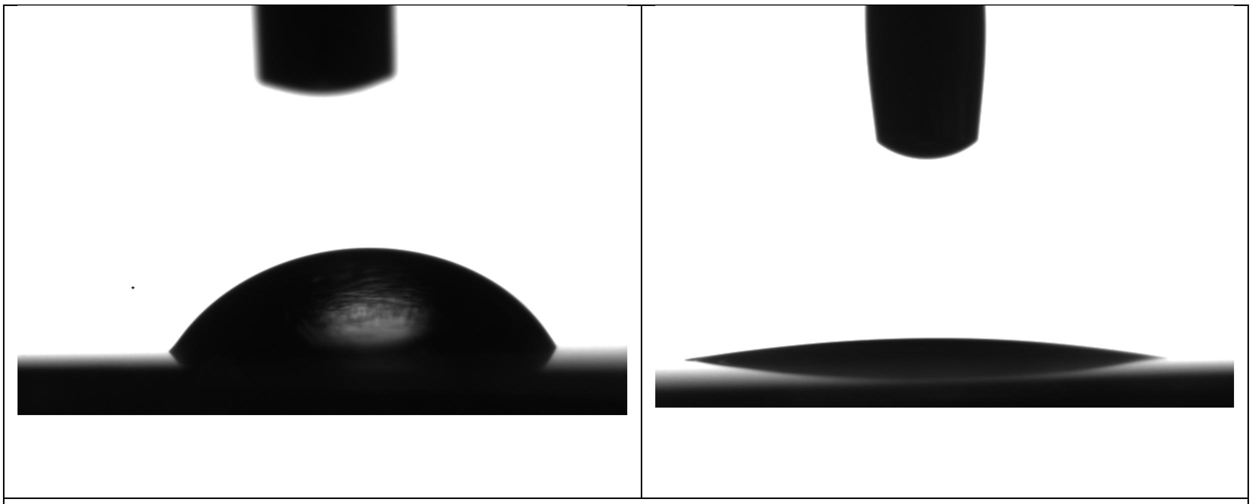

Figure A Image of Demi-water(Left) and NS-3(Right) droplet on the EOL element surface

The determined average surface free energy based on method described in section 3.2.2 are displayed in Table B.

Sample	σ_s [mN/m]	σ_s^P [mN/m]	σ_s^D [mN/m]
Element sample 1	40.13	6.05	34.08
Element sample 2	37.84	1.39	36.44

Table B Surface free energy and polar and dispersive components of the samples

Average contact angle of pulley sample

Average contact angles of four described lubricants on a pulley sample are presented in Table C. Furthermore, the screen shots of the contact angle for Demi-water and NS-3 are displayed in Figure B.

Sample	Average contact angle value over five measurements CA [°]			
	Diazomethane	**Ethylene glycol**	**Demi-water**	**NS-3**
Pulley	65.38	81.95	95.05	44.42

Table C Contact angle measurements of the samples

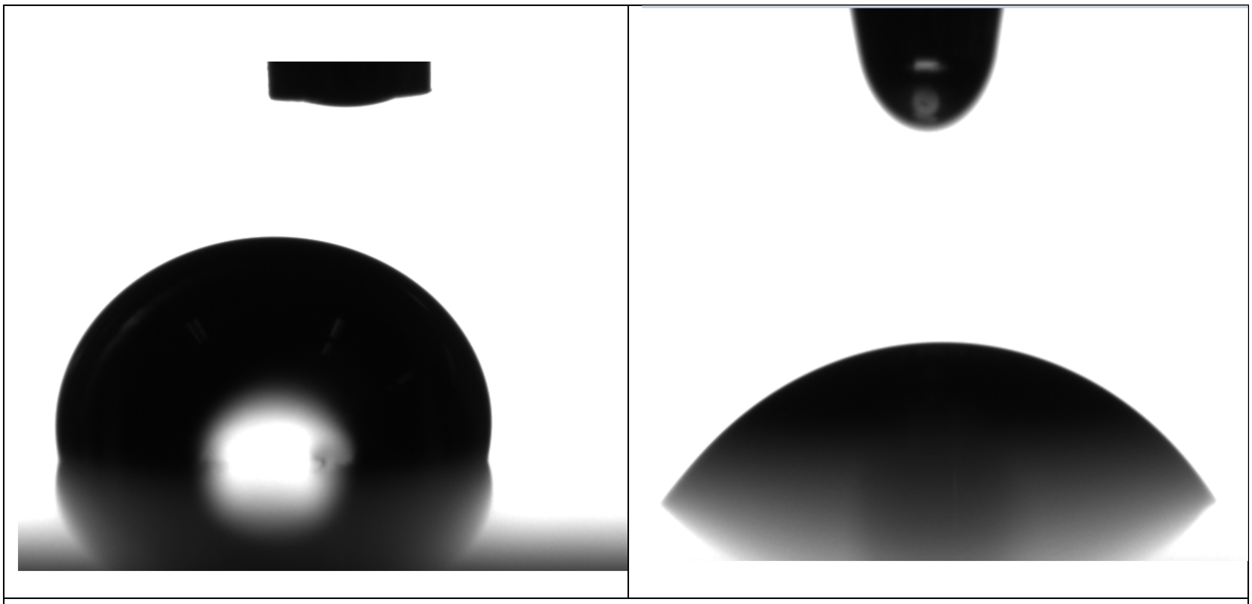

Figure B Image of Demi-water(Left) and NS-3(Right) droplet on the pulley surface

The determined average surface free energy based on method described in section 3.2.2 are displayed in Table D.

Sample	σ_s [mN/m]	σ_s^P [mN/m]	σ_s^D [mN/m]
Pulley	24.91	0.89	24.02

Table D Surface free energy and polar and dispersive components of the sample

Average contact angles of loop samples

Average contact angles of four described lubricants on the two nitrided and two non nitrided loop are for the inner surface presented in Table E and outer surface in Table F. Similarly, the screen shots of the contact angle for Demi-water and NS-3 are displayed in Figure C for inner surface and D for outer surface in case of non-nitrided loop surface. The screen shots of the contact angle for Demi-water and NS-3 for nitrided loop are displayed in Figure E for inner surface and F for outer surface respectively.

Sample	**Average contact angle value over five measurements CA [°]**			
	Diazomethane	**Ethylene glycol**	**Demi-water**	**NS-3**
Loop Non-Nitrided (Inside) sample 1	49.80	41.83	54.21	9.13
Loop Non-Nitrided (Inside) sample 2	48.32	43.63	58.00	-
Loop Nitrided (Inside) sample 1	49.19	47.13	70.44	6.18
Loop Nitrided (Inside) sample 2	52.60	51.92	71.52	-

Table E Contact angle measurements of the samples

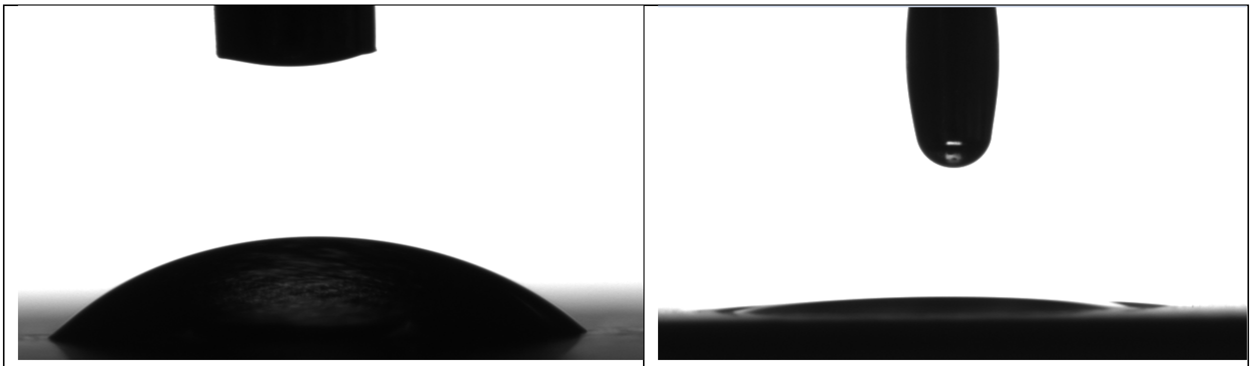

Figure C Image of Demi-water(Left) and NS-3(Right) droplet on the non nitrided loop inner surface

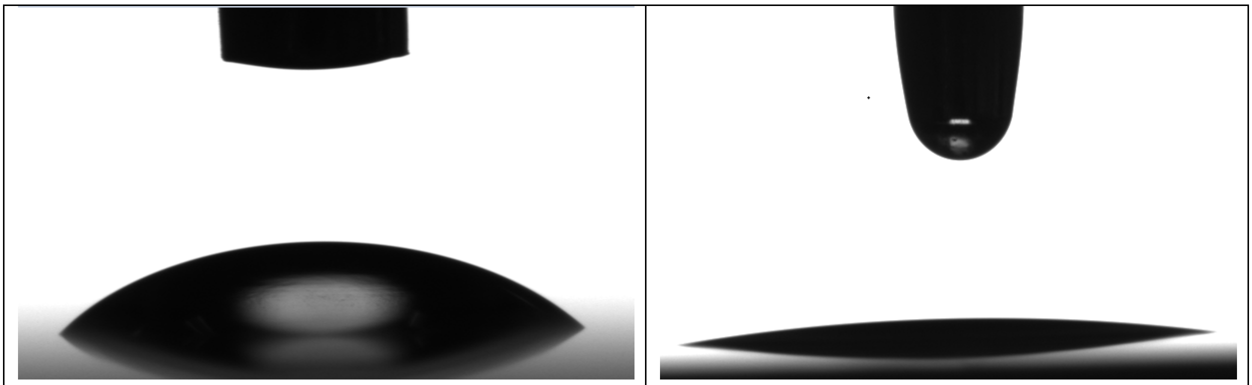

Figure D Image of Demi-water(Left) and NS-3(Right) droplet on the non nitrided loop outer surface

The determined average surface free energy based on method described in section 3.2.2 are displayed in Table F.

Sample	σ_s [mN/m]	σ_s^P [mN/m]	σ_s^D [mN/m]
Loop Non-Nitrided (Inside) sample 1	45.55	19.49	31.06
Loop Non-Nitrided (Inside) sample 2	44.30	12.12	32.18
Loop Nitrided (Inside) sample 1	40.26	6.76	33.49
Loop Nitrided (Inside) sample 2	38.00	6.79	31.21

Table F Surface free energy and polar and dispersive components of the samples

Sample	**Average contact angle value over five measurements CA [°]**			
	Diazomethane	**Ethylene glycol**	**Demi-water**	**NS-3**
Loop Non-Nitrided (Outside) sample 1	44.44	42.07	53.40	6.95
Loop Non-Nitrided (Outside) sample 2	47.66	43.93	55.14	-
Loop Nitrided (Outside) sample 1	48.74	46.38	61.87	9.17
Loop Nitrided (Outside) sample 2	51.60	44.88	62.27	-

Table G Contact angle measurements of the samples

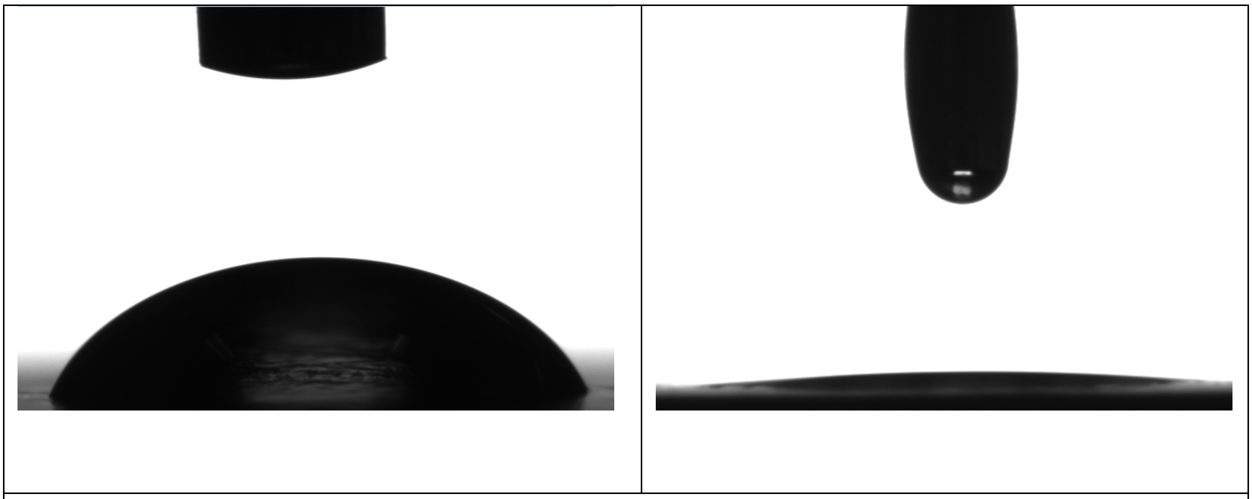

Figure E Image of Demi-water(Left) and NS-3(Right) droplet on the nitrided loop inner surface

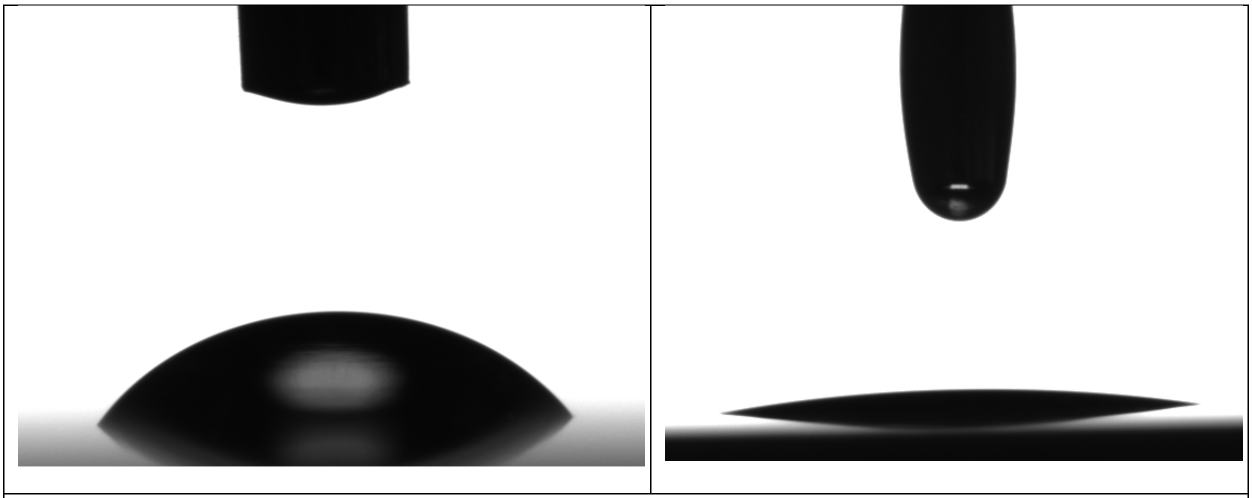

Figure F Image of Demi-water(Left) and NS-3(Right) droplet on the nitrided loop outer surface

The determined average surface free energy based on method described in section 3.2.2 are displayed in Table H.

Sample	σ_s [mN/m]	σ_s^P [mN/m]	σ_s^D [mN/m]
Loop Non-Nitrided (Outside) sample 1	46.84	13.30	33.54
Loop Non-Nitrided (Outside) sample 2	45.29	13.28	32.01
Loop Nitrided (Outside) sample 1	42.57	10.29	32.28
Loop Nitrided (Outside) sample 2	42.01	10.93	31.08

Table H Surface free energy and polar and dispersive components of the samples

Ethylene glycol and Demi-water surface plots for H* and D* respectively.

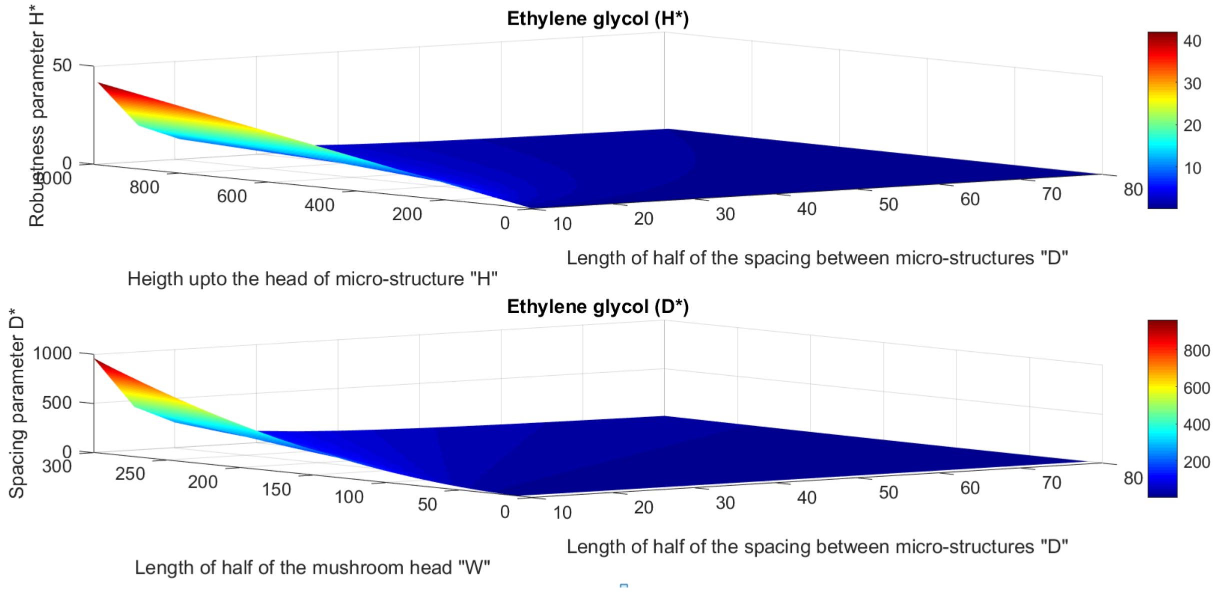

Figure G Surface plots representing parameters H and D* for Ethylene glycol*

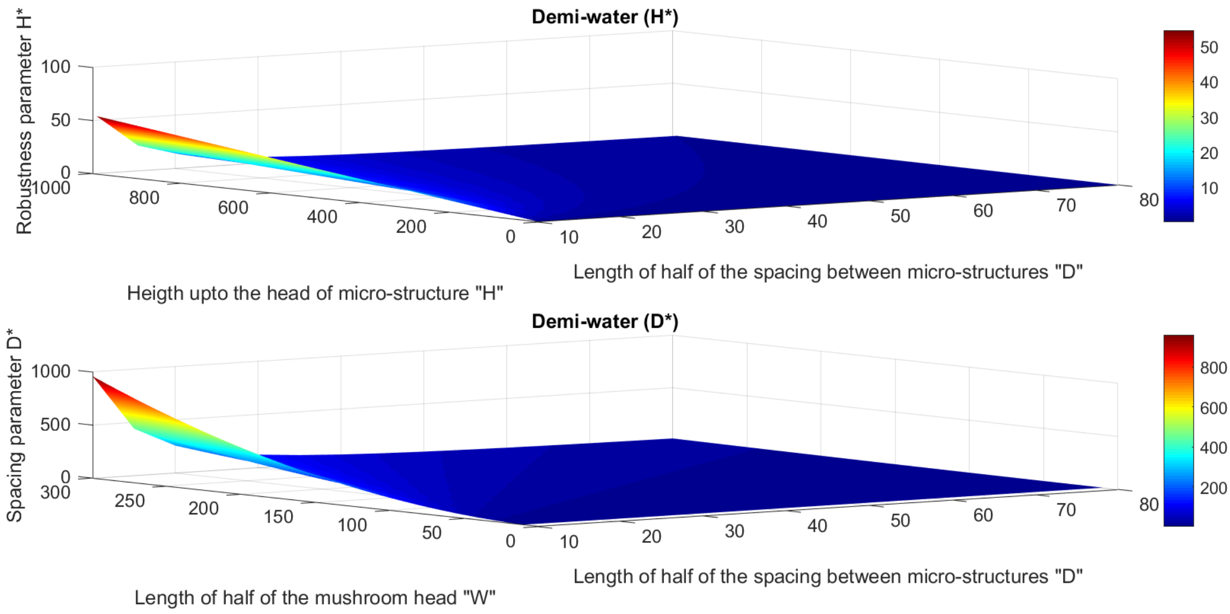

Figure H Surface plots representing parameters H and D* for Demi-water*

Ethylene glycol and Demi-water surface plots for apparent contact angle θ^* respectively.

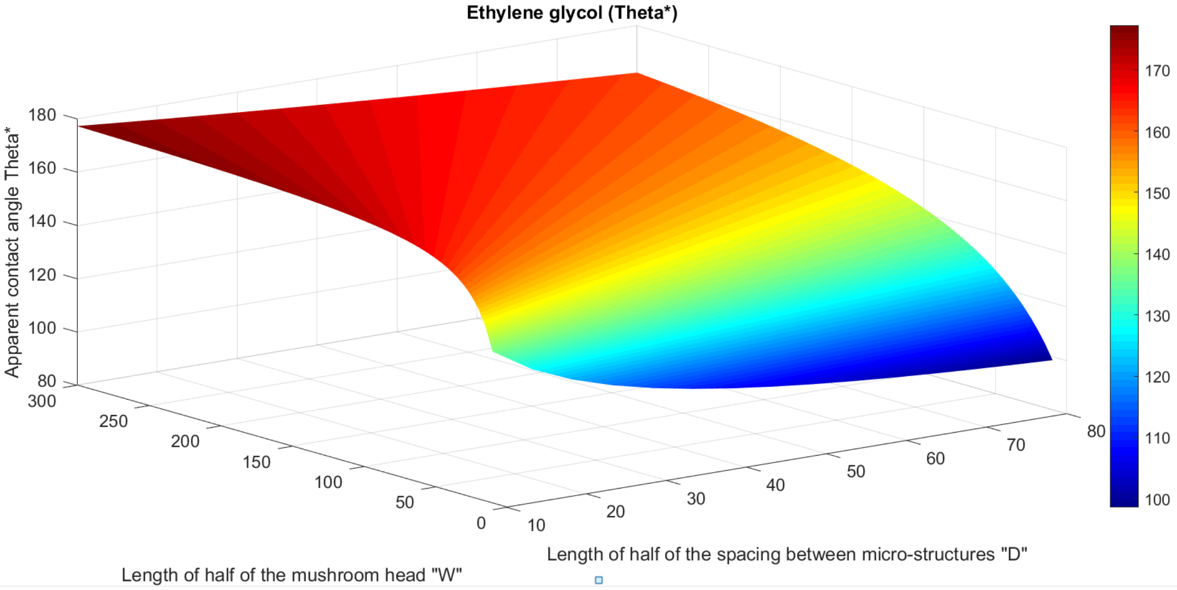

Figure I Surface plot of apparent contact angle for Ethylene glycol

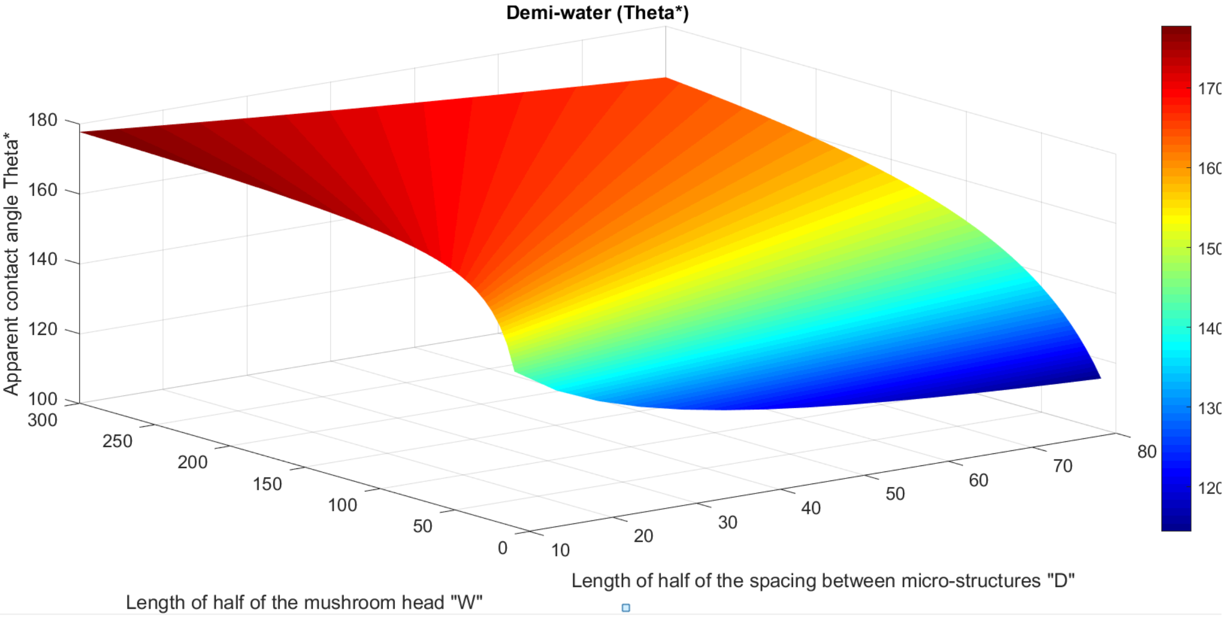

Figure J Surface plot of apparent contact angle for Demi-water